Simulating Frontal Low Level Jets and Quantifying their Impact on Wind Energy Production

Jori Dreef

Technische Universiteit Delft

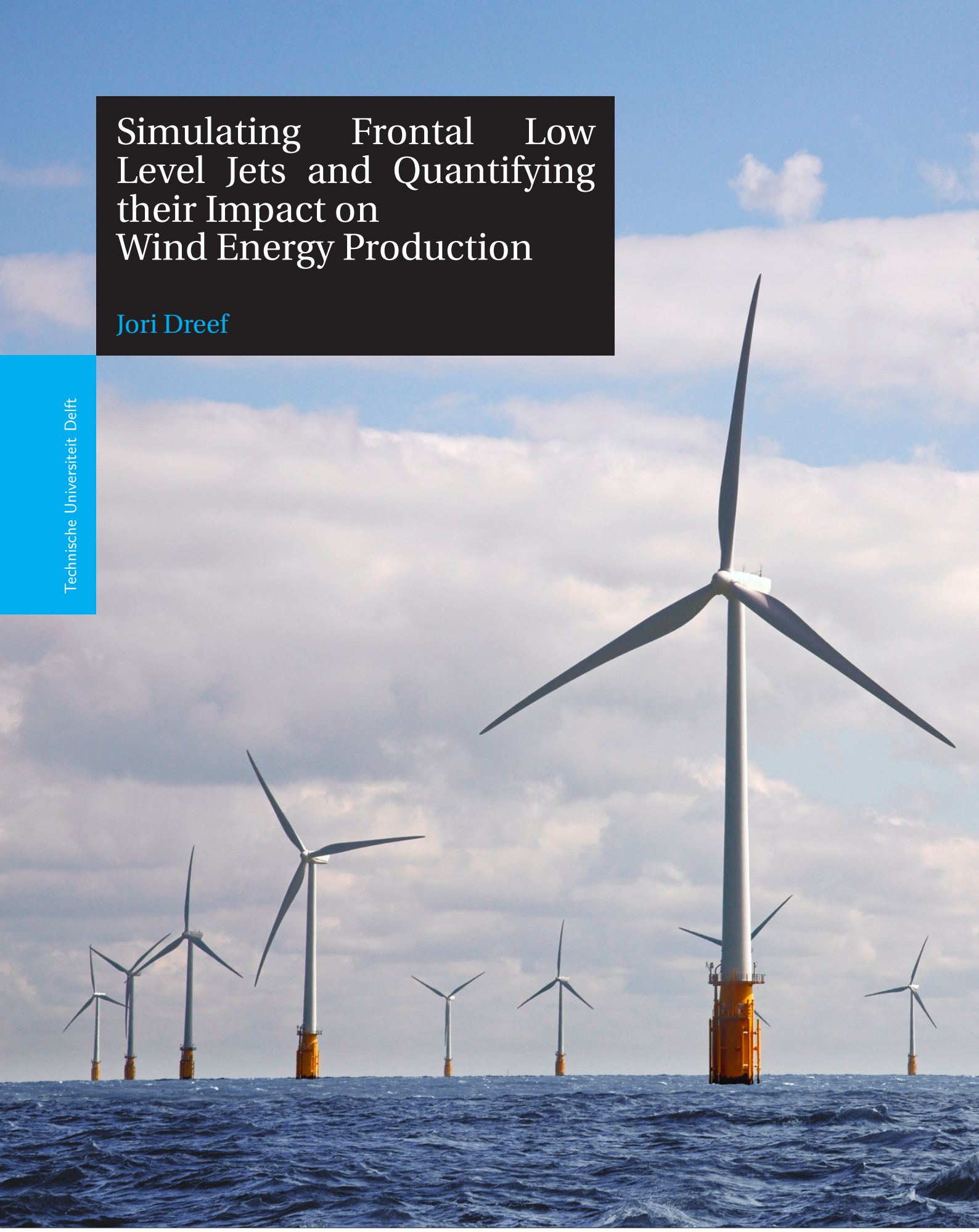

TU Delft Delft University of Technology

Challenge the future

Simulating Frontal Low Level Jets and Quantifying their Impact on Wind Energy Production

by

Jori Dreef

to obtain the degree of Master of Science
at the Delft University of Technology,
to be defended publicly on Thursday May 23, 2019 at 09:00 AM.

Student number:	4565215	
Project duration:	June 1, 2018 – May 23, 2019	
Thesis committee:	Dr. S. Basu,	TU Delft, supervisor
	J. Coelingh,	Vattenfall, supervisor
	Prof. dr. S. Watson,	TU Delft
	Prof. dr. H. J. J. Jonker,	TU Delft

An electronic version of this thesis is available at http://repository.tudelft.nl/.

TU Delft

ABSTRACT

Wind energy is becoming an important source of energy and reliable forecasts for the production of wind energy are needed to improve its integration in the power grid. The increasing height of wind turbines results in higher layers of the atmosphere being reached, where other phenomena than the surface-based ones can be of importance. One of these phenomena that can affect the wind energy production is a ramp up or a ramp down; a sudden increase or decrease in wind speed. One of the causes of a ramp down is a Frontal Low Level Jet (FLLJ), a jet stream which forms just ahead of a cold front. When the front has passed, the wind speed suddenly drops. It is yet unknown how well frontal Low Level Jets (LLJs) are simulated by a numerical weather prediction model.

For this research, case studies of occurrences of FLLJs were determined based on Light Detection And Ranging (LiDAR) observations, synoptic maps and coarse-resolution Weather Research and Forecasting (WRF) simulations. The chosen case studies were simulated with WRF using a finer resolution. These simulations were compared with surface observations from weather stations, wind profiler observations, LiDAR observations and observations from a wind farm.

From these comparisons it was concluded that the WRF model performed relatively well in general. The general development and dissolving of the FLLJ were simulated correctly, but the timing and magnitude of these simulations can be improved.

ACKNOWLEDGEMENTS

First of all, I want to thank Sukanta Basu for supervising my thesis throughout the last year. Whenever parts of my research didn't work out, he always had a new plan and was always available for a meeting or a short question. Second of all, I would like to thank Jan Coelingh for the opportunity to do my thesis with Vattenfall. This did not only allow me to work on a practical case, but also gave me some insight into how the wind energy industry works. I also would like to thank Simon Watson and Harm Jonker for taking place in my graduation committee and providing useful input during our meetings.

During my thesis, the 'wind simulation group' set up by Sukanta was a great help. The discussions and presentations were very informative and gave me useful ideas for my own research.

Moving from Wageningen to Delft a couple of years of ago was a bit more challenging than I expected, both academically and socially. However, I was lucky enough to have had an memorable time as a student in both cities and with two different groups of great people. I could not ask for a better start of my studies than the three years I had in Wageningen, thanks to the wonderful friends I made there. I'm also very grateful for my fellow GRS-students in Delft who made me feel welcome in a new city and who made my time as a student here very enjoyable. Especially the last year during my thesis I really enjoyed their company during the much needed coffee and lunch breaks. I would also like to thank everyone from Spartan and DDS for taking my mind off studying by providing me with a sporty distraction.

Finally, I would like to thank my parents and brother for their love, support and example.

Jori Dreef
Delft, May 2019

CONTENTS

List of Figures

List of Tables

List of Abbreviations

ABL	Atmospheric Boundary Layer
AWE	Airborne Wind Energy
CBL	Convective Boundary Layer
ECMWF	European Centre for Medium-Range Weather Forecast
EOWDC	European Offshore Wind Deployment Centre
FLLJ	Frontal Low Level Jet
FLS	Floating Lidar System
LiDAR	Light Detection And Ranging
LLJ	Low Level Jet
MY	Mellor-Yamada
MYJ	Mellor-Yamada-Janjic
MYNN2.5	Mellor-Yamada-Nakanishi-Niino2
N-S	Navier-Stokes
NWP	Numerical Weather Prediction
PBL	Planetary Boundary Layer
RANS	Reynolds-Averaged Navier-Stokes
TI	Turbulence Intensity
TKE	Turbulent Kinetic Energy
WRF	Weather Research and Forecasting
YSU	Yonsei University

NOMENCLATURE

ν	Kinematic viscosity [$m^2\ s^{-1}$]
ρ	Density [$kg\ m^{-3}$]
θ	Potential temperature [K]
A	Area [m^2]
C_P	Coefficient of power [-]
c_p	Specific heat capacity [$J\ kg^{-1}\ K^{-1}$]
F	Forcing term
f	Coriolis parameter [$rad\ s^{-1}$]
L_v	Latent heat [$J\ kg^{-1}$]
m	Model output of wind speed [$m\ s^{-1}$]
n	Number of observations [-]
o	Observations of wind speed [$m\ s^{-1}$]
P	Power [W]
p	Dynamic pressure [Pa]
q	Scalar flux
S_{q_t}	Stress term
t	Time [s]
u	Horizontal component of wind velocity [$m\ s^{-1}$]
v	Horizontal component of wind velocity (perpendicular to u)[$m\ s^{-1}$]
w	Vertical component of wind veloctiy [$m\ s^{-1}$]
x	Horizontal coordinate [m]
y	Horizontal coordinate (perpendicular to x) [m]
z	Vertical coordinate [m]

1

INTRODUCTION

The Earth's climate is changing due to human activity. Currently, humans have caused the global temperature to increase by 1.0° compared to pre-industrial levels. It is likely that this temperature rise will increase to 1.5° between 2030 and 2052 [Masson-Delmotte et al., 2018]. To reduce the emissions of greenhouse gasses, a rapid transition to renewable energy is needed [de Coninck et al., 2018]. Producing energy by using wind turbines is one of the ways to increase the amount of available renewable energy and to decrease the need for energy produced by fossil fuels. The amount of energy produced by wind turbines has been increasing and will keep increasing in the coming years. During 2017, 11.6% of the energy demand of the European Union was covered by wind power [Fraile and Mbistrova, 2017].

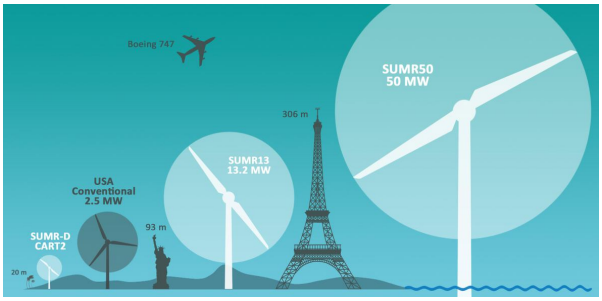

Figure 1.1: Increasing size of wind turbines [Loth et al., 2017].

Nowadays, wind turbines are almost competitive with coal and natural gas in terms of pricing [Zillmann and Bechtle, 2018]. To increase the power produced by one turbine and therefore to make it more cost efficient, the height and rotor size of turbines has to increase. The size of wind turbines has been increasing over the years and will keep increasing. Since 1985, the power of a single wind turbine has increased twentyfold [Loth et al., 2017]. Currently, turbines with blades of 200 meters length are being developed, resulting in turbines with a total tip height of almost 500 meters [Loth et al., 2017]. Although there seems to be a limit on how high wind turbines can be build, new inventions and research still provide opportunities for higher turbines with a larger rotor diameter [Loth et al., 2012]. The amount of energy produced by offshore wind turbines is higher than the amount of power produced by onshore wind turbines, but the latter ones are also a lot cheaper [Zillmann and Bechtle, 2018].

Figure 1.2: Kite used for wind energy production [Creighton, 2012].

Another trend is using kites or drones to capture wind (see figure 1.2). These systems are called Airborne Wind Energy (AWE) systems. A benefit of these systems is that there is no need for a tower or foundation which has to withstand the forces on the turbine [Zillmann and Bechtle, 2018]. Kites or drones would be cheaper to install and would produce more energy because they can reach heights where higher wind speeds can occur [Zillmann and Bechtle, 2018].

With an increase in size of (offshore) wind turbines or with AWE systems, higher layers of the atmosphere are reached. Here, different atmospheric phenomena than those occurring close to the surface could have effects on the load on wind turbines and the amount of energy they produce.

One of the current disadvantages of wind power is the uncertainty in the production forecast. A strong increase or decrease in wind speed over a short time period is called a ramp. Ramp-ups are usually caused by strong low pressure system, an Low Level Jet (LLJ), thunderstorms or other weather phenomena resulting in sudden strong winds [Sevlian and Rajagopal, 2013]. When these events reverse and the wind speed suddenly drops, a ramp down occurs. Being able to predict these peaks and dips in wind speed is important for knowing how much energy from other sources is needed [Ferreira et al., 2010, Sevlian and Rajagopal, 2013].

One of the causes of a wind ramp is an LLJ. The LLJ is a common atmospheric phenomena which has been studied extensively. An LLJ is a maximum in wind speed within the Atmospheric Boundary Layer (ABL). There are several causes for an LLJ. In this research the focus will be on a Frontal Low Level Jet (FLLJ), which is primarily caused by the passing of a cold front.

To study the effect of FLLJs on wind energy production, two case studies of the passing of these FLLJs are determined. The initial focus of this thesis was the wind farm in the bay of Aberdeen on the east side of Scotland. Several cases of FLLJs over this location could be determined with the help of Light Detection And Ranging (LiDAR) measurements, coarse-resolution Weather Research and Forecasting (WRF) model output, observations at a local weather station and wind profiles from a nearby weather radar/wind profiler. On the west side of Scotland, wind farm Edinbane is located on the Isle of Skye. This wind farm provided an opportunity to see the effects of FLLJs on the production of a wind farm. To do so, cases of FLLJs which pass over both Edinbane and Aberdeen have been determined.

My research will focus on the following questions:

1. What are the characteristics of the wind fields associated with FLLJs?
2. Can FLLJs and associated wind ramps be simulated reliably and how does this depend on the Planetary Boundary Layer (PBL) schemes?

In Chapter 2, a brief overview of the available literature on this subject will be given. In Chapter 3, the research itself and the used methods will be described. In Chapters 4 and 5, two case studies will be analysed. Lastly, in Chapter 6, lessons learned from this research and recommendations for future research will be given.

2

LITERATURE

2.1. WIND ENERGY CONVERSION

A wind turbine converts kinetic energy from the moving air into mechanical energy. Considering an airflow which passes through an area A with a wind speed v and a density ρ, the amount of kinetic energy P in this volume of air can be given by equation 2.1. Because mechanical energy is extracted from the flow, the wind speed behind the wind turbine will decrease, leading to the cross section of this flow to widen. The difference between the power before and behind the wind turbine is equal to the mechanical energy P_{mech} which is extracted from the air flow by the turbine and given by equation 2.2. In this equation A_1 and v_1 are the area and the wind speed before the wind turbine, A_2 and v_2 are the area and the wind speed behind the wind turbine [Hau, 2006]. The non-dimensional power coefficient C_p of a wind turbine is given by equation 2.3 [Hau, 2006, Viré, 2018]. The power coefficient represents the fraction of the total power which is extracted from the airflow by the wind turbine [Hau, 2006]. The maximum, and therefore ideal, power coefficient is 0.59. This coefficient is called the the Betz limit. This is the case when $v_2/v_1 = 1/3$ [Hau, 2006].

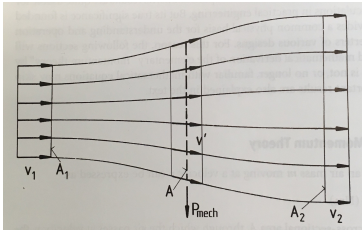

Figure 2.1: Wind flow before and after a wind turbine (located at the arrow P_{mech}) [Hau, 2006].

$$P = \frac{1}{2} \cdot \rho \cdot A \cdot v^3 \tag{2.1}$$

$$P_{mech} = \frac{1}{2} \cdot \rho \cdot (A_1 \cdot v_1^3 - A_2 \cdot v_2^3) \tag{2.2}$$

$$C_P = \frac{P_{mech}}{P} \tag{2.3}$$

The characteristics of a wind turbine can be described by a power curve and a plot of the power coefficient. In figures 2.2a and 2.2b, these characteristics are given for the wind turbine of the type Enercon E70. These will be of importance further on in this thesis. Above a wind speed of about 15 m s^{-1} the generated power no longer increases. This is the rated wind speed. Above a wind speed of 25 m s^{-1}, the turbine is turned off and the generated power becomes zero. This is the cut-out wind speed [Viré, 2018]. The maximum C_p for this turbine is about 0.5, which is lower then the Betz limit.

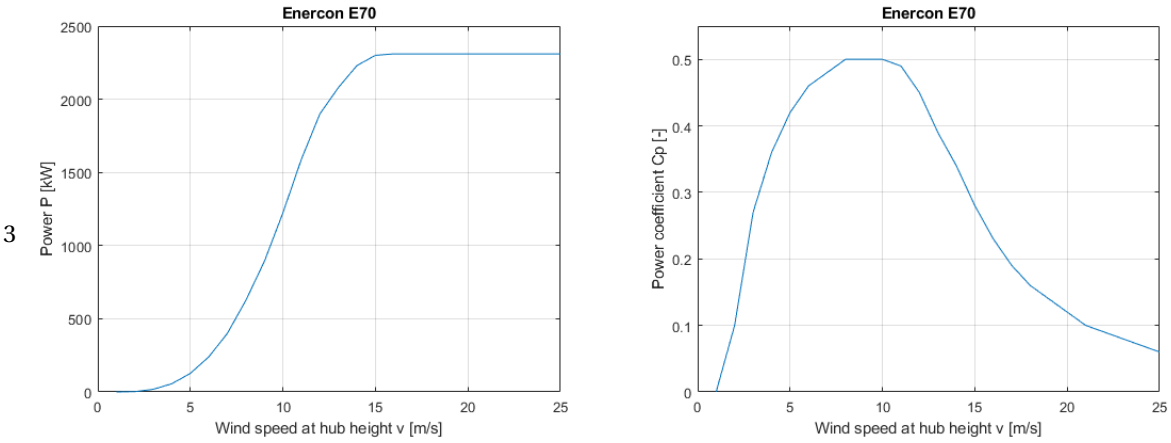

(a) Power curve

(b) Power coefficient

Figure 2.2: Characteristic of an Enercon E70 turbine.

2.2. WIND RAMPS

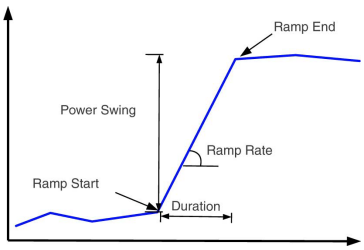

Figure 2.3: Time series of a wind ramp with time on the x-axis and power on the y-axis [Sevlian and Rajagopal, 2013].

One of the current disadvantages of wind power is the uncertainty in the production prediction. A strong increase or decrease in wind speed over a short time period is called a ramp (see figure 2.3). Ramp downs occur less often than ramp ups on average [Kamath, 2010]. Being able to predict these fluctuations in wind speed is important for knowing how much energy from other sources is needed [Sevlian and Rajagopal, 2013]. In case of a ramp up, the generation of energy from other sources has to be decreased. When a ramp down occurs, the generation of energy from other sources has to be increased [Kamath, 2011]. Usually, the wind energy forecast is based on meteorological data from measurement towers, combined with weather models. Research from Kamath [2011] has shown that wind speed related variables, temperature and humidity are the most important variables needed from meterological data. Wind energy production forecasts are made a couple of hours ahead and updated hourly [Kamath, 2011]. A more accurate wind generation forecast and a better understanding of wind ramps leads to better management of the intermittent nature of wind resources [Kamath, 2010]. This research will only focus on LLJs as a cause of ramp downs.

2.3. LOW LEVEL JETS

The LLJ is a common atmospheric phenomena which has been studied extensively. An LLJ is a sudden increase in wind speed within the ABL. There is no strict definition of LLJ. Andreas et al. [2000] defines it as a local maximum in wind speed which is 2 m s^{-1} higher that the wind speeds above and below it (see figure 2.4).

There are several causes for an LLJ, but all of them come down to a disturbance of the balance of forces, causing the upper-level wind to decouple from the surface. Most of these disturbances depend on diurnal variations and/or characteristics of the surface [Andreas et al., 2000, Banta et al., 2002, Doyle and Warner, 1991, Parish, 2000].

A well-known case of the LLJ is the nocturnal LLJ. During the day, the boundary layer consists of a mixed layer in which turbulence occurs and the wind speed is almost constant with height. During the night, the surface cools and a stable boundary layer forms in the lowest part of the mixed layer. The upper remainder of the mixed layer (now called the residual layer) therefore becomes decoupled from the surface and is no longer affected by friction [Andreas et al., 2000, Baas et al., 2009, Banta et al., 2002, Blackadar, 1957, Doyle and

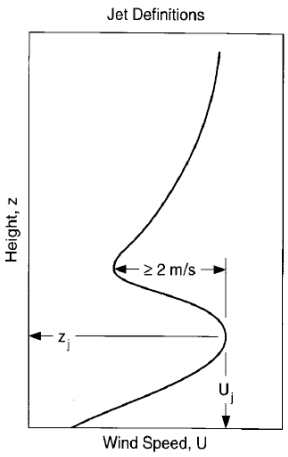

Figure 2.4: Ideal wind profile in case of a LLJ [Andreas et al., 2000].

Warner, 1991, Parish, 2000, Shapiro and Fedorovich, 2010, Storm et al., 2009, Thorpe and Guymer, 1977]. This decoupling leads to an imbalance in the overall force balance, which results in an inertial oscillation enabling the wind speed in this flow to increase [Blackadar, 1957].

2.4. FRONTAL LOW LEVEL JETS

A lesser studied cause of an LLJ is that of the FLLJ. Occurrences of FLLJs over the British Isles have been observed by Browning and Harrold [1970]. Jets parallel to the cold front, around the location of the surface front were observed. Several FLLJs which were observed by Browning and Pardoe [1973] all roughly followed the same pattern (see figure 2.5). Just ahead of the front, a FLLJ occurs at around 900 mb. Behind the cold front, the main tropospheric jet is located a lot higher at around 300 mb. The wind speeds reached in the latter FLLJ are usually higher than those in the FLLJ ahead of the front. Just ahead of the surface front, warm air is ascending, causing a lot of forced convection [Browning and Harrold, 1970]. The risen air then splits into a forward and a backward flow, relative to the surface cold front. The rearward flow is ascends because it passes over the cold front, the forward flow descends. Both of these flows are capped by a layer of dry air. The backward flow is also capped from underneath by the upper layer of the cold front which is moving in. These air motions cause heavy precipitation at the location of the cold front at the surface, and stratiform precipitation after the passing of the cold front. The reversed horizontal temperature gradient just in front of the cold front causes a decrease in the geostrophic wind near the top of the Convective Boundary Layer (CBL). This results in a jet stream at lower heights (see figure 2.6) [Browning and Pardoe, 1973].

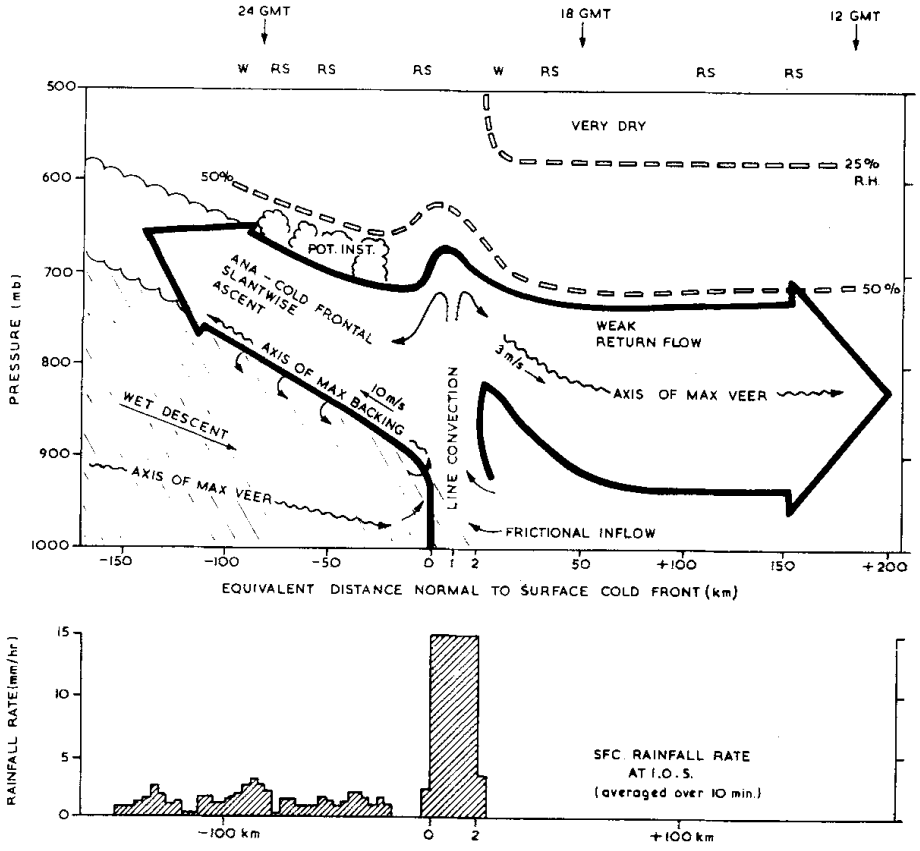

Figure 2.5: Observations of air motions around a frontal passage [Browning and Pardoe, 1973].

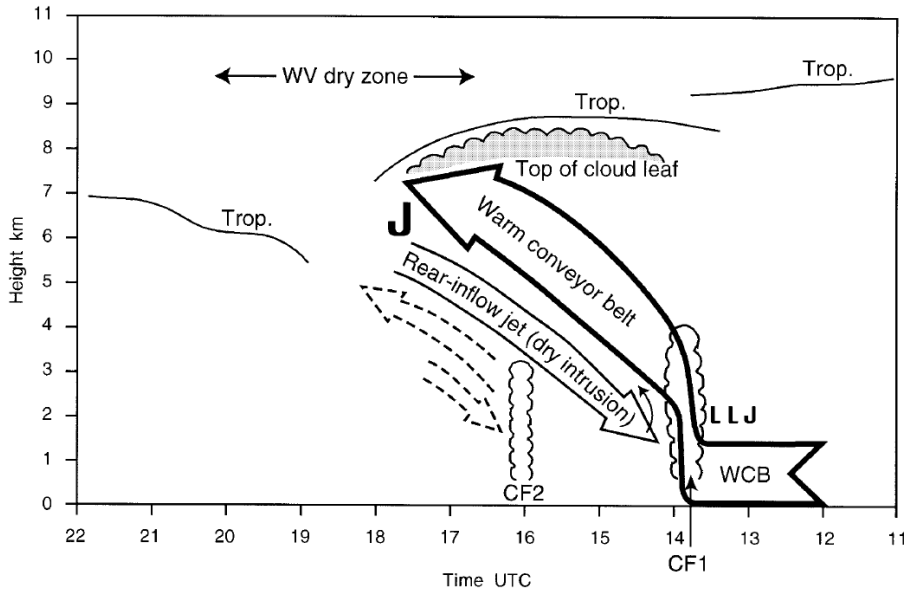

Figure 2.6: Schematic cross section of a FLLJ [Browning et al., 1998].

2.4.1. COLD FRONTS

A front is a boundary between air masses. Characteristics of fronts include enhanced temperature and moisture gradients, a strong vertical wind shear and ascending air, clouds and precipitation. The intensity of a front is highest near the surface and decreases with increasing altitude. For this thesis, the main focus will be on cold fronts. In general, the passing of cold fronts is advanced by a cold air mass and brings showers and thunderstorms. But the passing of a cold front can also be accompanied by dry, clear sky [Lackmann, 2011]. Behind a cold front, usually moderate precipitation occurs for a period of time [Browning and Harrold, 1970]. Cold fronts can be classified as a katafront or a anafront. At a katafront, precipitation occurs ahead of the front, while at an anafront, precipitation occurs at the back side of the front [Lackmann, 2011]. In katafronts, there is hardly any ascent in the warm conveyor belt along the front. Instead, dryer, cooler air moves ahead of the cold front [Lackmann, 2011]. With an anafront, air will be lifted by cold air. When precipitation is falling through this layer of cold air, precipitation in the form of snow or ice can occur. Observations in the central U.S. showed anafronts to be often accompanied by a southerly FLLJ but this might also be the case in other parts of the world [Lackmann, 2011].

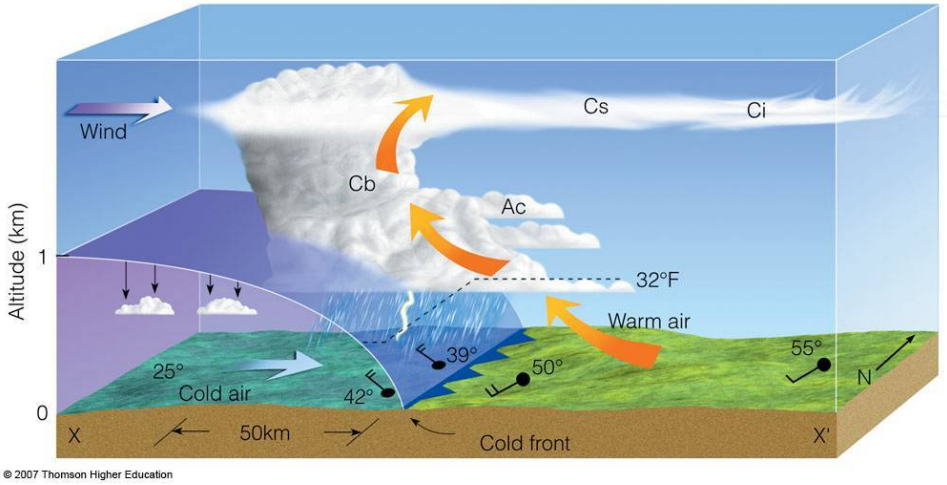

Figure 2.7: Cold front [Thomson, 2007].

2.5. PLANETARY BOUNDARY LAYER PARAMETRISATIONS

Numerical Weather Prediction (NWP) models are models which are based on mathematical equations to describe the motion and flow of fluids. Because of computational limits, the atmosphere cannot be represented perfectly, but is represented by a grid of points. When the grid resolution increases, the structure of the atmosphere is represented better. Currently, some atmospheric phenomena which influence the large scale flows are too small to be represented correctly by NWP models. To include the effects of these phenomena, parametrisation schemes are used in NWP models. A parametrisation scheme is the relation between the sub-grid process represented by the parametrisation schemes and the known model variables [Stensrud, 2007]. To model turbulence, the Reynolds-Averaged Navier-Stokes (RANS) equations (see equation (2.6) till (2.7)) are used. The horizontal terms for the fluxes are neglected in these equations. The equations are derived by applying Reynolds averaging on the Navier-Stokes (N-S) equations. The N-S equations (2.4) are a set of equations to model turbulence accurately. The terms of equation 2.4 describe, from left to right, the inertia, the advection, the pressure gradient force, viscous stress and forcing. Reynolds averaging is decomposing variables in a mean and a fluctuating part [Stensrud, 2007]. An example of this can be seen in equation (2.5). The term $\overline{a'b'}$ represents the influence of the eddy motions [Stensrud, 2007]. Equations (2.8) and (2.9) the used equations for the scalar fluxes.

$$\frac{\partial u_i}{\partial t} + \frac{\partial (u_i u_j)}{\partial x_j} = -\frac{1}{\rho}\frac{\partial p}{\partial x_i} + \nu \frac{\partial^2 u_i}{\partial x_j \partial x_j} + F_i \tag{2.4}$$

$$\overline{A \cdot B} = \overline{(\overline{A} + a')(\overline{B} + b')} = \overline{\overline{A}\overline{B} + \overline{A}b' + \overline{B}a' + a'b'} = \overline{A}\overline{B} + \overline{a'b'} \tag{2.5}$$

$$\frac{\partial \overline{u}}{\partial t} + \overline{u}\frac{\partial \overline{u}}{\partial x} + \overline{v}\frac{\partial \overline{u}}{\partial y} + \overline{w}\frac{\partial \overline{u}}{\partial z} - f\overline{v} = -\frac{1}{\overline{\rho}}\frac{\partial \overline{p}}{\partial x} - \frac{\partial \overline{u'w'}}{\partial z} \tag{2.6}$$

$$\frac{\partial \overline{v}}{\partial t} + \overline{u}\frac{\partial \overline{v}}{\partial x} + \overline{v}\frac{\partial \overline{v}}{\partial y} + \overline{w}\frac{\partial \overline{v}}{\partial z} - f\overline{u} = -\frac{1}{\overline{\rho}}\frac{\partial \overline{p}}{\partial y} - \frac{\partial \overline{v'w'}}{\partial z} \tag{2.7}$$

$$\frac{\partial \overline{q}}{\partial t} + \overline{u}\frac{\partial \overline{q}}{\partial x} + \overline{v}\frac{\partial \overline{q}}{\partial y} + \overline{w}\frac{\partial \overline{q}}{\partial z} = -\frac{S_{q_t}}{\overline{\rho}} - \frac{\partial \overline{q'w'}}{\partial z} \tag{2.8}$$

$$\frac{\partial \overline{\theta}}{\partial t} + \overline{u}\frac{\partial \overline{\theta}}{\partial x} + \overline{v}\frac{\partial \overline{\theta}}{\partial y} + \overline{w}\frac{\partial \overline{\theta}}{\partial z} = -\frac{1}{\overline{\rho} c_p}\frac{\partial F}{\partial z} - \frac{L_v}{\overline{\rho} c_p} - \frac{\partial \overline{\theta'w'}}{\partial z} \tag{2.9}$$

The last term of each of equation 2.6 to 2.9 is the Reynolds term. These terms are unknown and a closure scheme is needed to establish them. With these equations, there will always be more unknowns than equations. The problem of always having more unknowns than equations is known as the turbulence closure problem. These unknown terms can be parametrised by relating them to known variables. There are several closure schemes to solve this problem. These schemes can be categorised in different orders of closure. First order closure schemes provide equations for the state variables u, v, w, T, q or the first moments and a parametrisation for the covariance terms. Second order closure schemes provide equations for the state variables and the covariance terms and a parametrisation for the triple correlation terms. [Stensrud, 2007]

First-order closure scheme (K-closure) In a first-order closure scheme, the prognostic equations for the means of variables are preserved and the turbulent fluxes are parametrised [Skamarock et al., 2008]. It uses a flux-gradient relation and solves the problem of the unknown covariances to that of specifying the eddy diffusivities [Garratt, 1994].

The Yonsei University (YSU) scheme The Yonsei University (YSU) scheme is a non-local closure scheme [Hu et al., 2010]. This scheme is classified as a first-order closure scheme. To account for entrainment processes at the top of the PBL, an asymptotic entrainment flux term is included [Shin and Hong, 2011]. The YSU scheme has proven to perform well in simulating convection related to a cold front [Hong et al., 2006].

1.5-order closure scheme In a 1.5-order closure scheme, not only equations for the standard prognostic variables ($\overline{u}, \overline{v}, \overline{\theta}, \overline{q}$) are included, but for the potential temperature variance ($\overline{\theta'^2}$) and the Turbulent Kinetic Energy (TKE) ($\overline{e}$) as well [Stensrud, 2007]. This scheme relates diffusivity directly to the turbulent intensity [Garratt, 1994].

The Mellor-Yamada-Janjic (MYJ) scheme The Mellor-Yamada-Janjic (MYJ) scheme is classifed as a local closure scheme. The scheme determines eddy diffusion coefficients from prognostically calculated TKE. It uses the 1.5 order turbulence closure (also called TKE closure) model to represent turbulence above the surface layer [Hu et al., 2010, Shin and Hong, 2011].

Second-order closure scheme The second-order closure scheme elaborates on the 1.5-order closure scheme by also including predictive equations for all the remaining covariance terms [Stensrud, 2007]. These covariances are evaluated by solving their rate equations [Garratt, 1994].

The Mellor-Yamada-Nakanishi-Niino-2 (MYNN2.5) scheme The MYNN2.5 scheme is an improvement of the Mellor-Yamada (MY) scheme by Nakanishi and Niino [Nakanishi and Niino, 2004, 2006]. Because it does not solve the prognostic equations for several variables, the computational costs are lower compared to the Mellor-Yamada scheme [Nakanishi and Niino, 2004]. This scheme has demonstrated to be an improvement on the MY with regards to the representation of several phenomena, amongst which are coastal barrier jets [Olson et al., 2019].

2.6. WIND FARM PARAMETRISATION

A wind farm can have an effect on local winds, turbulence and temperature downwind [Fitch et al., 2012]. To account for the effect of a wind farm in an atmospheric model, wind farm parametrisation needs to be used. In this case, the wind farm parametrisation proposed in Fitch et al. [2012] is used. When using this parametrisation, the wind farm is modelled as a momentum sink, transferring kinetic energy into electricity and TKE. The type of turbine is taken into consideration since the thrust coefficient is used to calculate the total amount of kinetic energy which is extracted from the wind by the turbine. Because the power coefficient, which quantifies the fraction of the kinetic energy which is converted into electrical energy is known, the remaining kinetic energy which is converted into TKE is known [Fitch et al., 2012]. The effect of this wind farm parametrisation can be seen in figure 2.8. CTRL is the control run with a wind farm on coordinates (0,0), NF is the run without a wind farm. The negative values for the wind speed in the left plot show that the control run models the wind speed downwind of the wind farm lower than the run without a wind farm. The right plot of the TKE shows that the control run models the wind farm as a source of TKE.

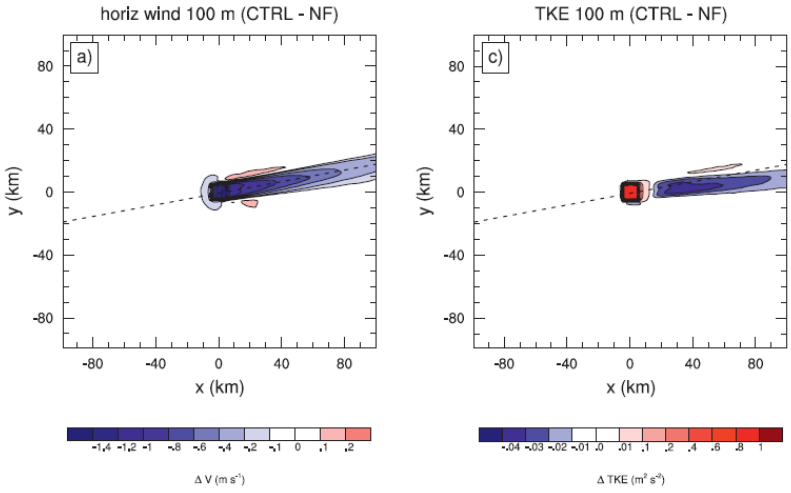

Figure 2.8: The result of wind farm parametrisation in WRF [Fitch et al., 2012].

2.7. LIDARS

A LiDAR determines the distance (range) from an object to the device itself by measuring the time it takes an emitted pulse to go back and forth. A LiDAR uses wavelengths which are visible to the human eye [Donovan, 2018]. There are several types of LiDAR which can be used for atmospheric research but only Doppler wind LiDARs measure wind speeds, so this research will focus on that type of LiDAR [Emeis, 2011].

There are a few methods to determine the range by using Doppler LiDAR. First, the range can be determined by measuring the signal delay. Secondly, it is possible to use beam focusing to determine the range. Lastly, the range can be determined by using optical coherence tomography [Emeis, 2011].

A Floating Lidar System (FLS) consists of a LiDAR mounted to a buoy. FLSs were introduced as a tool for offshore wind resource assessment since they are cheaper and easier to install than a mast with meteorological measurement devices (met mast). With a FLS, also the motions of the buoy have to be monitored in order to correct the wind speed and wind direction measurements for this. FLSs which are currently available are able to measure up to about 200 m [Gottschall et al., 2017].

3

METHODS

3.1. OBSERVATIONS

This study focusses on two different areas in Scotland where different observation measurements are available. An overview of all the measurement locations can be found in Appendix A. A close up of the measurement locations around the Edinbane area can be found in figure 3.1 and that of the Aberdeen area can be found in figure 3.2.

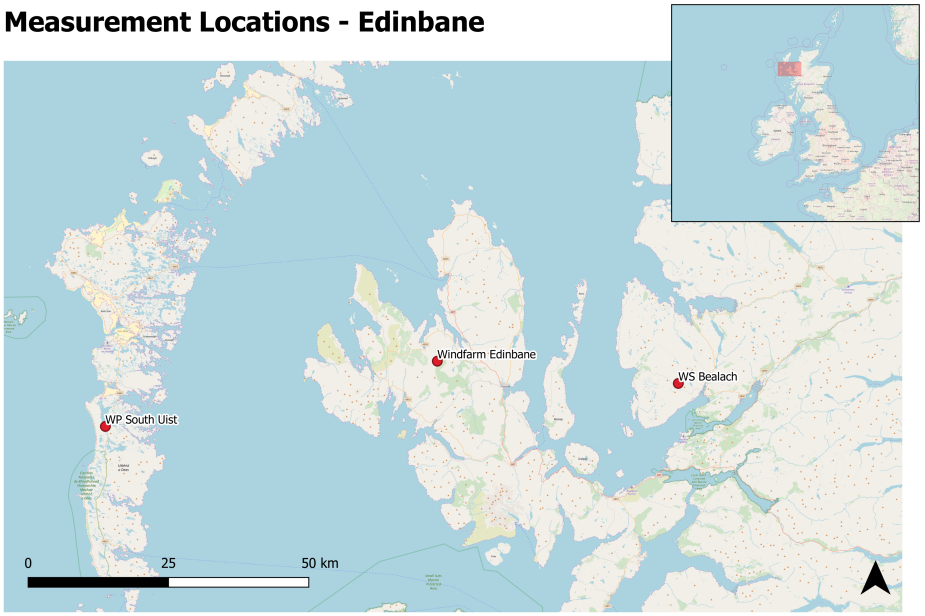

Figure 3.1: Measurement locations at Edinbane, United Kingdom.

3.1.1. SURFACE OBSERVATIONS

Bealach Na Ba weather station The Bealach Na Ba weather station is an automatic weather station from the Met Office. This weather station is located about 42 kilometres east of wind farm Edinbane at an altitude of 773 meters [MetOffice, 2018]. The weather station is located on the edge of a cliff (see pictures in Appendix B)Among the available measurements are wind speed, wind direction and temperature.

Dyce weather station The Dyce weather station is an automatic weather station from the Met Office. This weather station is located at the airport of Aberdeen, about 12 kilometres west of wind farm Aberdeen, at an

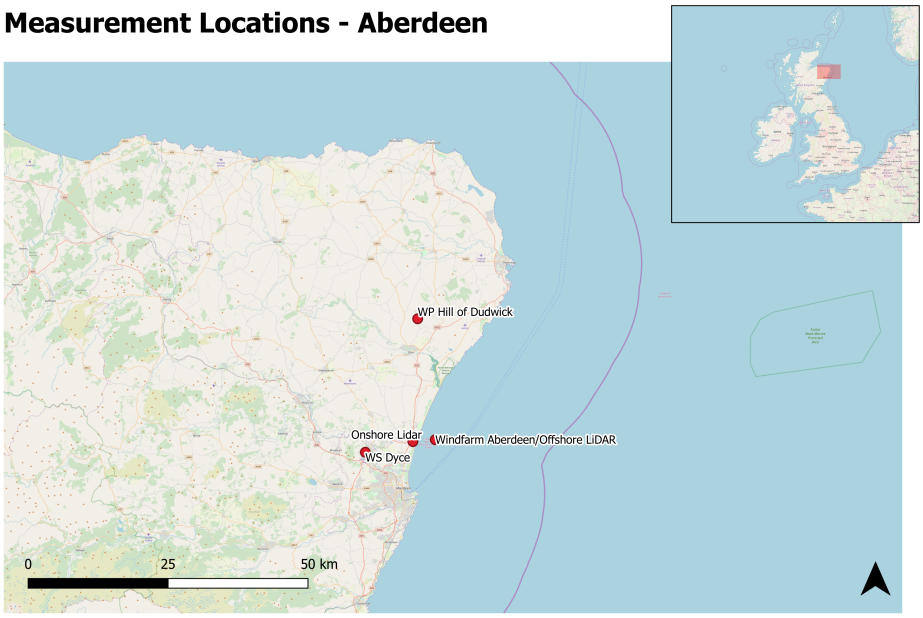

Figure 3.2: Measurement locations at Aberdeen, United Kingdom.

altitude of 65 meters [MetOffice, 2018]. Among the available measurements are wind speed, wind direction, temperature and pressure.

3.2. UPPER AIR OBSERVATIONS

Hill of Dudwick weather radar/wind profiler The weather radar at Hill of Dudwick is a C-band radar. A C-band radar has a wavelength between 4 and 8 centimetres and a range between 100 and 130 kilometres [Unal, 2018]. This radar is located about 21 kilometres north of the wind farm at Aberdeen.

Figure 3.3: C-band radar at Hill of Dudwick [Speight, 2014].

South Uist Wind Profiler At the island of South Uist a wind profiler is located. It is located about 60 kilometres west of wind farm Edinbane. This profiler is able to provide wind measurements up to 20 kilometers.

Aberdeen LiDAR The LiDARs used during the measurement campaign as part of the wind resource assessment at the location of the future wind farm in the bay of Aberdeen are both from ZephIR. The distance between the two LiDARs is about 4 kilometres [Baker, 2016, White, 2016].

Floating LiDAR The LiDAR was deployed on November 1st 2016. There is data from November 2016 till January 2018 which is averaged over 10 minutes. At every measurement height, packets (number of samples included in 10-min average), wind direction, horizontal wind speed, vertical wind speed, horizontal standard deviation, vertical standard deviation, lowest horizontal wind speed, highest horizontal wind speed are measured. The height configurations of the LiDAR are different during some months but for most of the time the measurements are taken at heights of 17 m, 38 m, 58 m, 82 m, 99 m, 124 m, 140 m and 181 m. The measurement at 38 m is used as reference [ZephIR, 2012]. In November 2016, the logger on the buoy failed so only the data from the LiDAR itself is available. In June 2017, the LiDAR itself failed but data from the buoy itself might be available. From July 6, 2017 till August 25, 2017, measurements were performed at other heights because of wrong settings after a check up visit. Besides information about the wind, also data about the waves is logged. For every 10 minutes, the average heading, pitch, roll and heading is available.

Land-based LiDAR The land-based LiDAR measured at 8 different heights: 23 m, 38 m, 64 m, 88 m, 105 m, 130 m, 146 m and 187 m. At every height the wind direction, horizontal wind speed, lowest horizontal wind speed, highest horizontal wind speed, horizontal standard deviation wind speed, vertical wind speed and Turbulence Intensity (TI) are measured. The LiDAR was installed on September 9, 2016 and from that day till January 23, 2018 consistent measurements are available. After that day the power failed and new batteries were installed on January 30, 2018. Then the data was logged again from January 31, 2018 till March 5, 2018. Then there is inconsistent data until May 8, 2018.

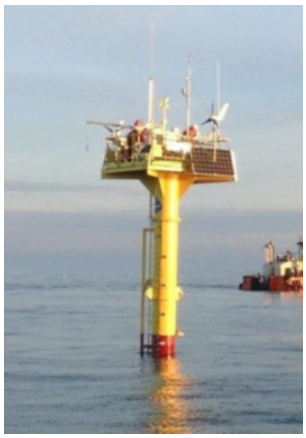

Figure 3.4: The FLS used in this research [White, 2016].

3.3. WIND FARMS

The Edinbane wind farm is located on the isle of Skye in the Northwest of Scotland. The wind farm consists of 18 2.3 MW turbines with a hub height of 64 meters and has an total installed capacity of 41.4 MW [Hutchinson, 2014]. The farm has been operational since 2010. The wind farm at Edinbane consists of 18 wind turbines of the type Enercon E70. The power curve of these wind turbines was already shown in figure 2.2a on page 4. For this wind farm, the wind power production data is available every 10 minutes.

In the bay of Aberdeen, the European Offshore Wind Deployment Centre (EOWDC) is located. This wind park is a relatively new offshore wind test and demonstration facility and supplies energy to the city of Aberdeen. The wind park consists of 11 wind turbines which will produce 312 GWh per year [Vattenfall, 2016]. The turbines are of the type V164 with a tip height of 191m and a blade length of 80 m [Ghazi, 2018]. The total capacity of the wind farm will be 93.2 MW [Vattenfall, 2016].

3.4. MODELLING

For this research, WRF version 3.9.1.1 was used. 4 domains were used, with a resolution of 27 km, 9 km, 3 km and 1 km respectively. A map of the domains can be found in Appendix C. Three different combinations of PBL schemes and wind farm parametrisation were tested:

- YSU PBL scheme
- Mellor-Yamada-Nakanishi-Niino2 (MYNN2.5) PBL scheme
- MYNN2.5 PBL scheme + wind farm parametrisation

Details on these PBL schemes and the wind farm parametrisation can be found in section 2.5 and 2.6. As initial conditions and boundary conditions, the European Centre for Medium-Range Weather Forecast (ECMWF) Interim Reanalysis (ERA-Interim) data is used. As microphysics scheme, the WRF single-moment 5-class system was used. A single-moment scheme only predicts the mixing ratio of particles. Schemes that predict this mixing ratio and the concentration of particles are called double-moment schemes. Double-moment schemes perform better in a large range of environmental conditions, while multiple different single-moment schemes are needed for this [Stensrud, 2007].

3.5. DETERMINING CASE STUDIES

To determine cases of LLJs, the data from the LiDARs was used. By looking at time-height plots for every day, some potential cases of FLLJs could be determined. Since the measurement height of the LiDARs was limited to 200 meters, other data was needed to conclude on the case studies. For the potential cases, a month long WRF run with a low resolution was performed. 3 domains were used, with resolutions of 27 km, 9 km and 3 km respectively. The YSU PBL scheme and grid nudging were used. This was done for the months of February, June and November in 2017. This allowed the amount of potential cases to be narrowed down. In figure 3.5, the wind speed at the location of the offshore LiDAR in Aberdeen for every day of November is plotted. At a substantial amount of days, local increases in wind speed occur, which could be considered to be LLJs. These increases last for a couple of hours and then dissolve. However, some of these increase dissolve very abruptly, for example on the 7th and the 16th of November. When the synoptic maps (figure 3.6a and 3.6b) for these

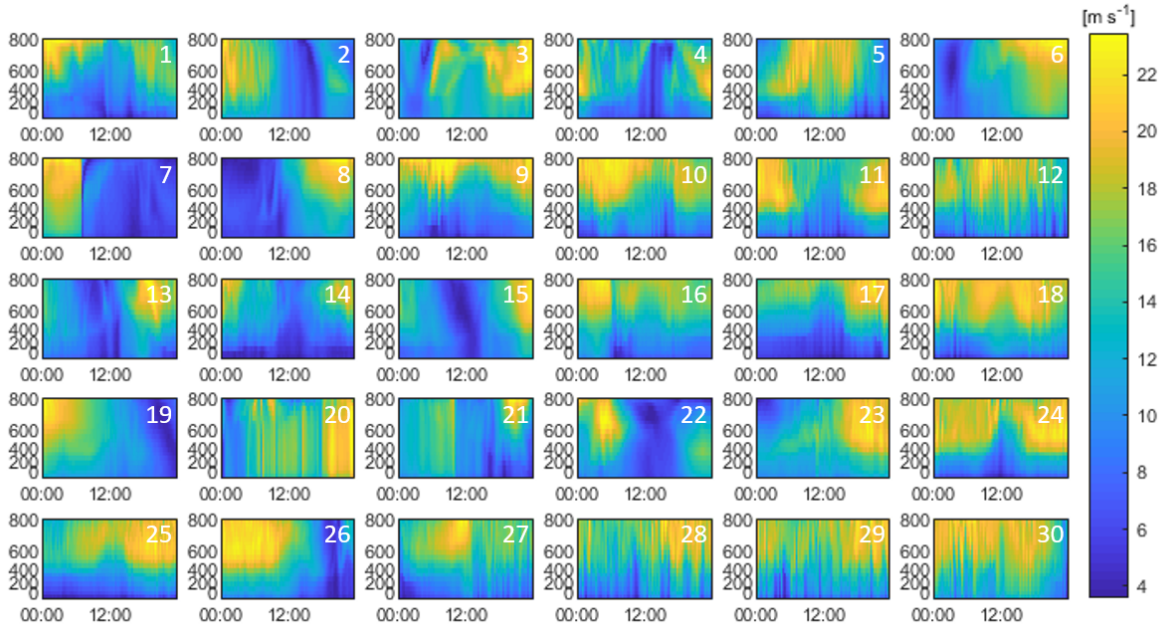

Figure 3.5: Time-height plots of WRF output at the location of the offshore LiDAR for every day in November 2017.

days were studied, these abrupt decreases in wind speed corresponded with the passing of a cold front. This lead to the conclusion that these LLJs are FLLJs.

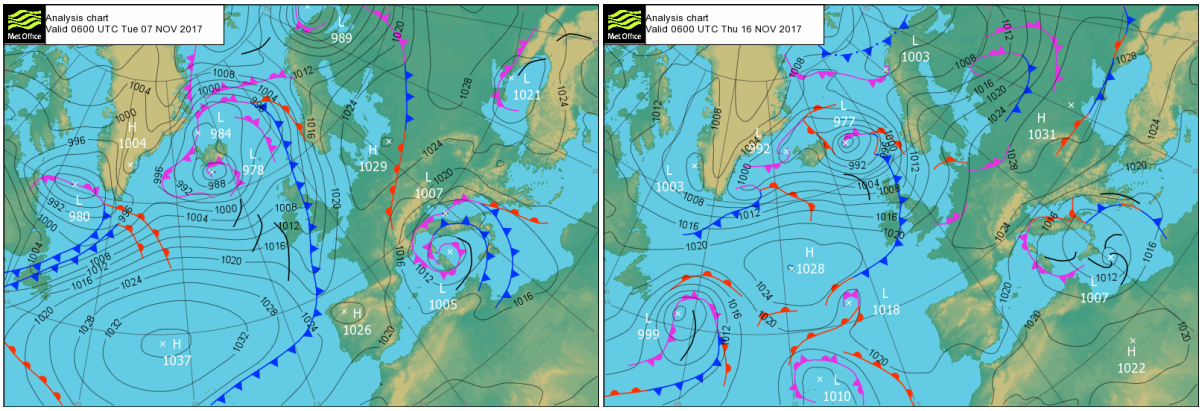

(a) Synoptic map of 0600 UTC, November 7, 2017 [MetOffice, 2017b].

(b) Synoptic map of 0600 UTC, November 16, 2017 [MetOffice, 2017b].

Figure 3.6: Synoptic maps for potential case studies.

4

CASE STUDY I

The first case study that will be investigated is the passing of a cold front over Scotland during the 6th and 7th of November, 2017.

4.1. SYNOPTIC SITUATION

During the 6th and 7th of November, a cold front slowly moved over Ireland and the United Kingdom. As can be seen in figure 4.1a, this cold front was just south of wind farm Edinbane at the Isle of Skye around 18 UTC at the 6th of November. Around 7 UTC on the 7th of November the cold front passed over the bay of Aberdeen (see figure 4.1b).

During the passing of this cold front, there was a classic situation of a strong Icelandic Low and a strong Azores High. This synoptic situation results in higher temperatures than usual in southern and eastern Europe, rain and colder weather over the British Isles and alternating weather over the countries in between [Vogan, 2016]. The Icelandic Low steers mid-latitude cyclones over the British Isles and Northern Europe [Stull, 2017]. An Icelandic Low and a strong Azores High can cause an 'atmospheric river'; a band of precipitation which lays over the United Kingdom.

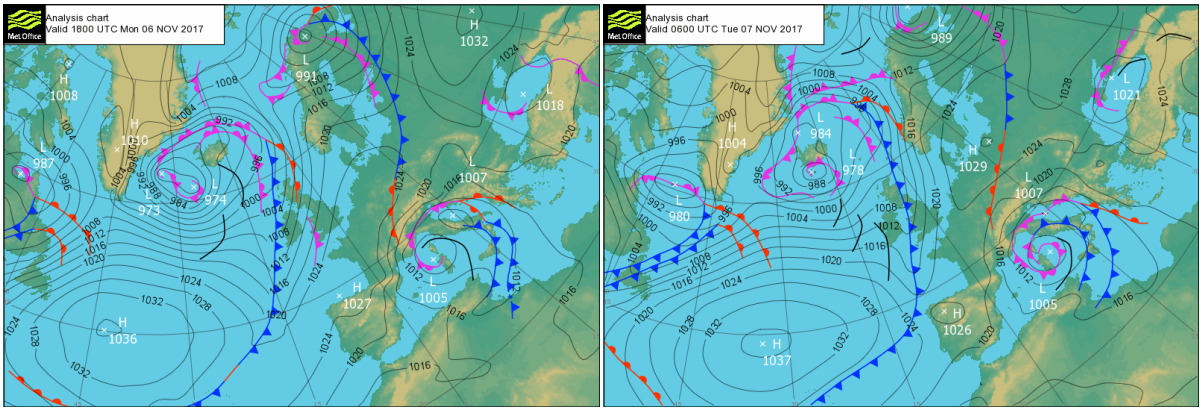

(a) Synoptic map of 1800 UTC, November 6, 2017 [MetOffice, 2017b].

(b) Synoptic map of 0600 UTC, November 7, 2017 [MetOffice, 2017b].

Figure 4.1: Synoptic maps for Case Study I.

4.2. RADAR AND SATELLITE OBSERVATIONS

As can be seen in figure 4.2a, a line of precipitation is laying over the sea north west of Scotland around 12 UTC. This is the precipitation which corresponds with the cold front.

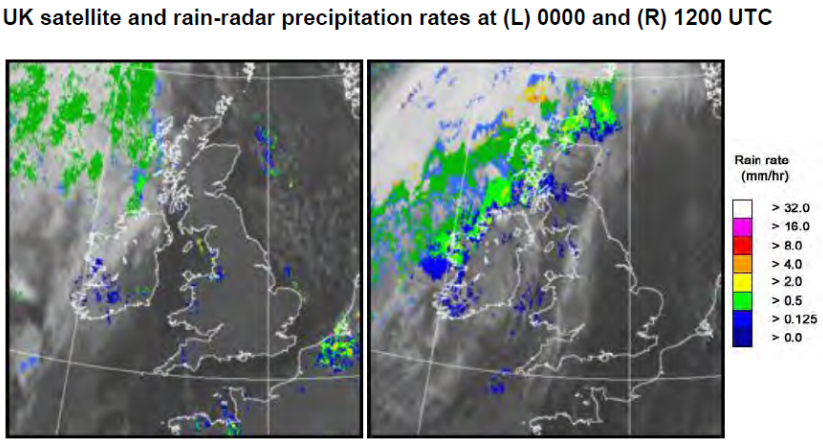

(a) Precipitation radar measurements at 00 UTC and 12 UTC at November 6, 2017 [MetOffice, 2017a].

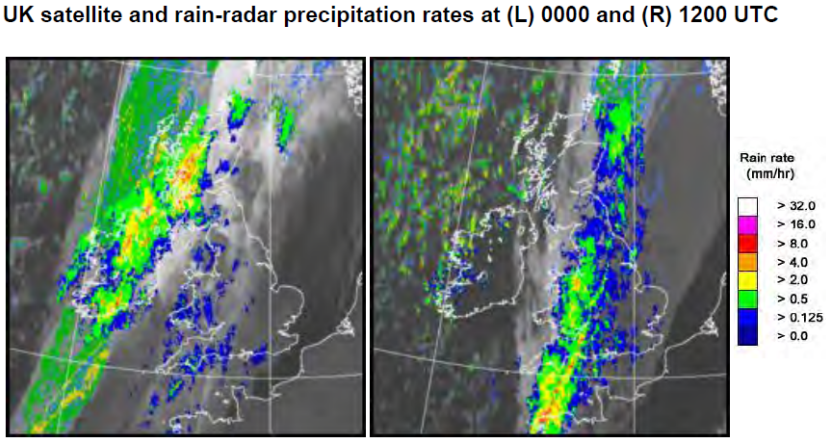

(b) Precipitation radar measurements at 00 UTC and 12 UTC at November 7, 2017 [MetOffice, 2017a].

Figure 4.2: Radar images for Case Study I.

4.3. SURFACE OBSERVATIONS

The wind speed measured by the weather stations from the MetOffice at 10m height are shown in figure 4.3a and figure 4.3b for Edinbane and Aberdeen respectively. The measurements for Edinbane show a clear drop in wind speed after the cold front passes. At Aberdeen, also a drop in wind speed is visible, although this is less drastic. In figure 4.3c the means sea level pressure for Aberdeen is plotted. This also shows a sudden change in trend in the pressure when the cold front passes. Unfortunately, no pressure data from Edinbane is available.

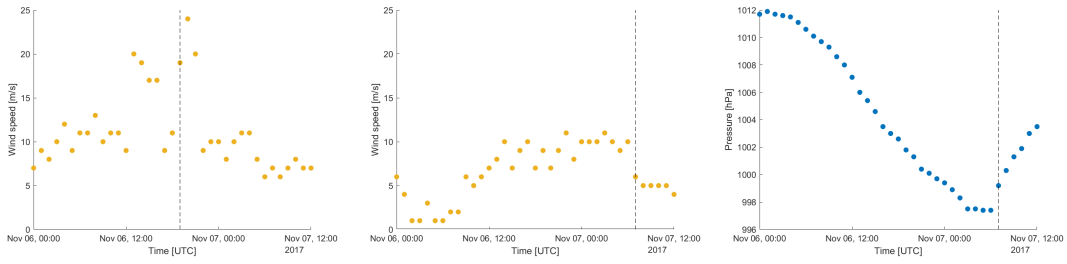

(a) Wind speed measurements at Edinbane. (b) Wind speed measurements at Aberdeen. (c) Mean sea level pressure at Aberdeen.

Figure 4.3: Surface measurements from MetOffice weather stations.

4.4. UPPER AIR OBSERVATIONS

The data from wind farm Edinbane also shows the passing of the cold front. The measurements shown in figure 4.4a and figure 4.4b show a sudden drop in both the wind speed at hub height and therefore the generated power. It should be noted that the wind speed at the surface (figure 4.3a) is higher than the wind speed at hub height (figure 4.4a). This could indicate a measurement error in one of the data sets.

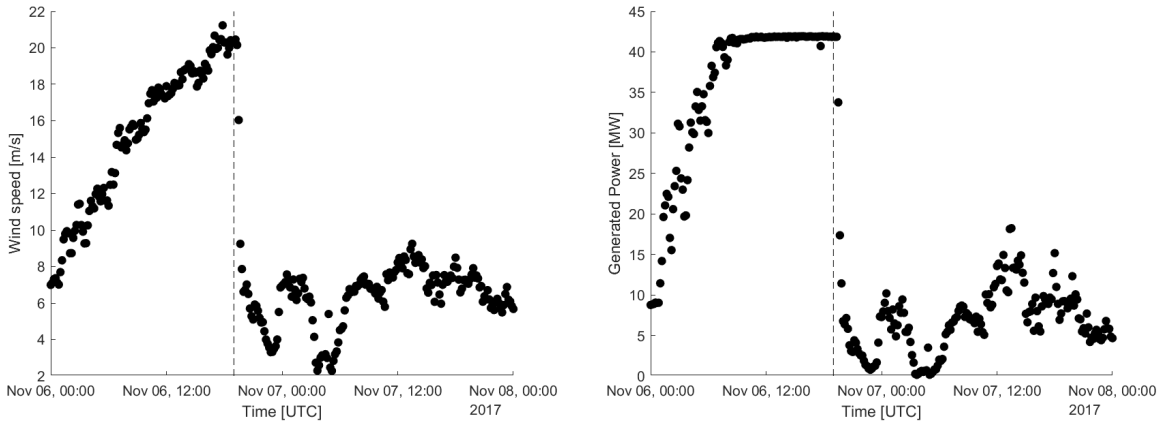

(a) Wind speed at hub height at wind farm Edinbane.

(b) Generated power at wind farm Edinbane.

Figure 4.4: Measurements at hub height at wind farm Edinbane.

The measurements from the wind profiler at South Uist start around a 1000 meters and go up till 15 kilometres. As can be seen in figure 4.5, the wind speed at an altitude of 1000 meters drops from 25 m s^{-1} to 10 m s^{-1} in a little over an hour.

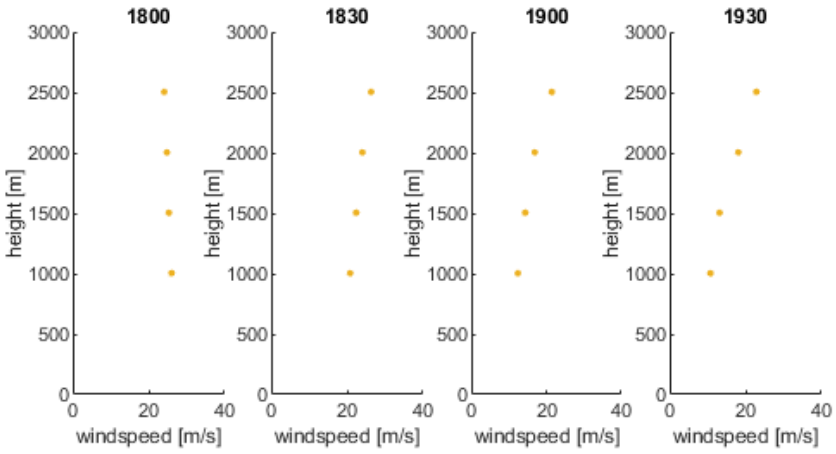

Figure 4.5: Wind profiler measurements at South Uist on November 6.

The measurements from the offshore LiDAR, the onshore LiDAR and the wind radar/wind profiler at Hill of Dudwick can be seen in figure 4.6. The wind profiler only has measurements above 200 meters and the LiDAR only measure up to 200 meters. The LiDARs clearly show a sudden decrease in wind speed in the lower part of the atmosphere.

From the available LiDAR measurements at Aberdeen, a time-height plot (figure 4.7) can be made. These measurements show the development of a FLLJ around 1700 UTC, November 6. This FLLJ persists through the night and quickly dissolves around 0700 UTC, November 7.

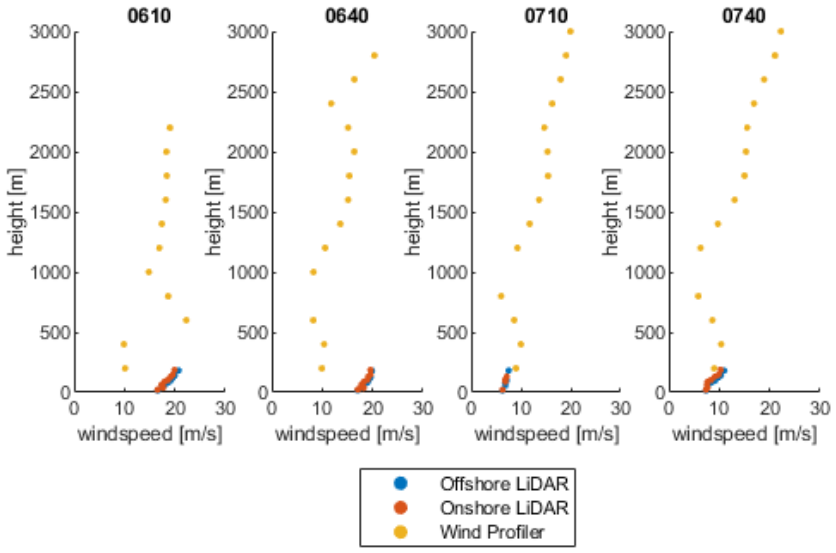

Figure 4.6: Wind profiler measurements over Hill of Dudwick and offshore LiDAR measurements over Aberdeen on November 7.

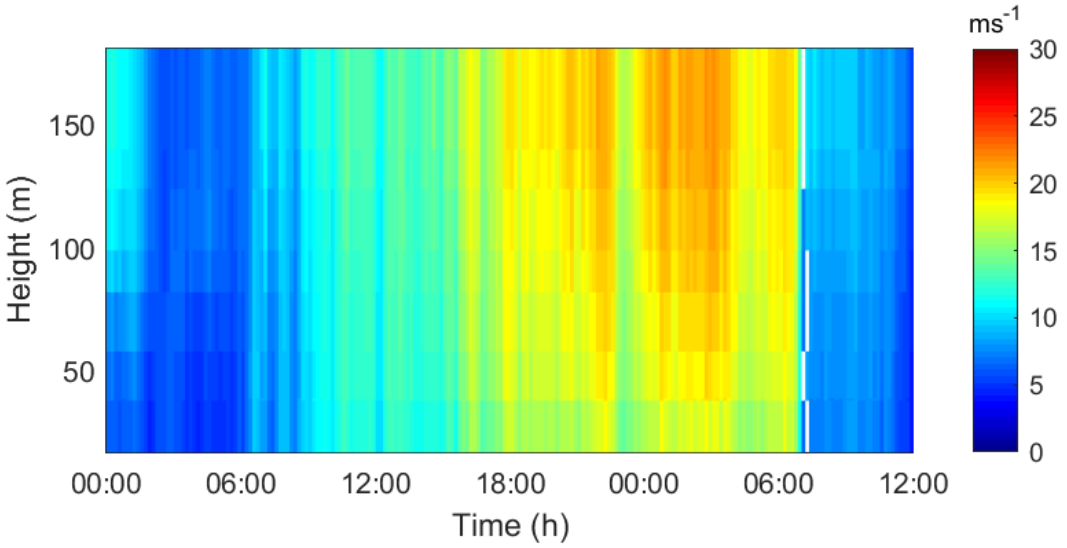

Figure 4.7: Offshore LiDAR observations from 0000 UTC, November 6 till 1200 UTC, November 7, at Aberdeen.

4.5. MESOSCALE MODELLING

In figure 4.8 the wind speed measured by the weather station and wind park, and the wind speeds modelled by the different WRF simulations are shown. When looking at figure 4.8a the wind speed simulated by WRF at the surface is lower than the observations of the weather station at that location. The WRF simulation does show an increase in wind speed when the cold front is passing over, but not as strong as the measurements show. In figure 4.8b the wind speed at hub height is plotted. The WRF outputs from all three runs agree with the observations from the wind park for the first 12 hours. After about 12 hours, the wind speed from WRF suddenly drops, while the observed wind speed keeps increasing. Just after the observed wind speed suddenly drops, the wind speed from WRF peaks again. After this peak, the observations and the model output seem to roughly agree. The 2D wind speed maps (Appendix D, F, E and G) show that the cold front is simulated moving back an forth. The simulated FLLJ therefore passes two times over Edinbane, explaining the

sudden decrease and increase in wind speed. The maps of simulated surface winds for 1900 UTC, November 6 (Appendix D (YSU) and F (MYNN2.5 + WP) show that the wind speed is higher in the YSU map than in the MYNN2.5 + WP map. In all simulations, the structure of the FLLJ is visible. Just before the cold front, the wind direction is parallel to the front. After the front passes, the wind direction is perpendicular to the cold front itself. There is also an abrupt decrease in temperature by a couple of degrees.

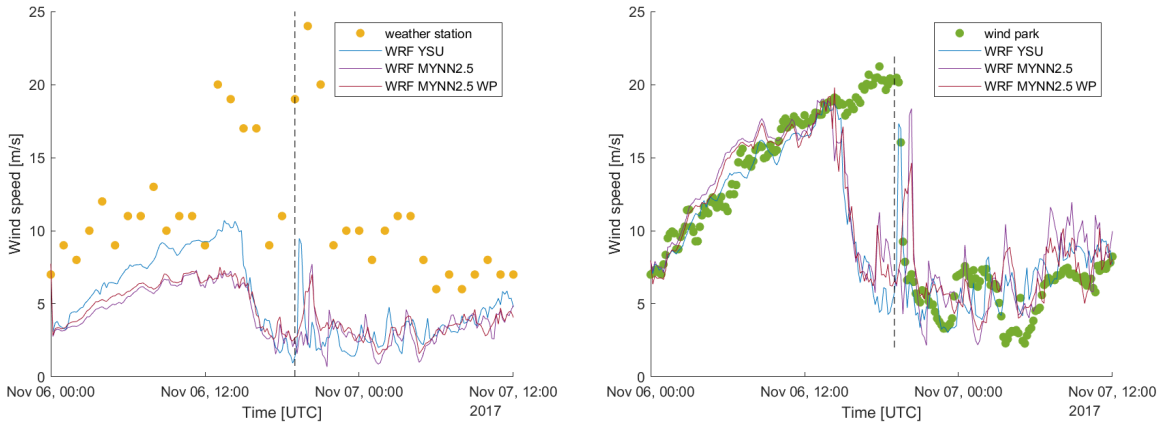

(a) Surface height (10m).

(b) Hub height (64m).

Figure 4.8: Wind speed measurements and WRF output over Edinbane

$$RMSE = \sqrt{\frac{1}{n}\sum_{j=1}^{n}(p_j - o_j)^2} \tag{4.1}$$

$$NRMSE = \frac{\sqrt{\frac{1}{n}\sum_{j=1}^{n}(p_j - o_j)^2}}{\overline{o}} \tag{4.2}$$

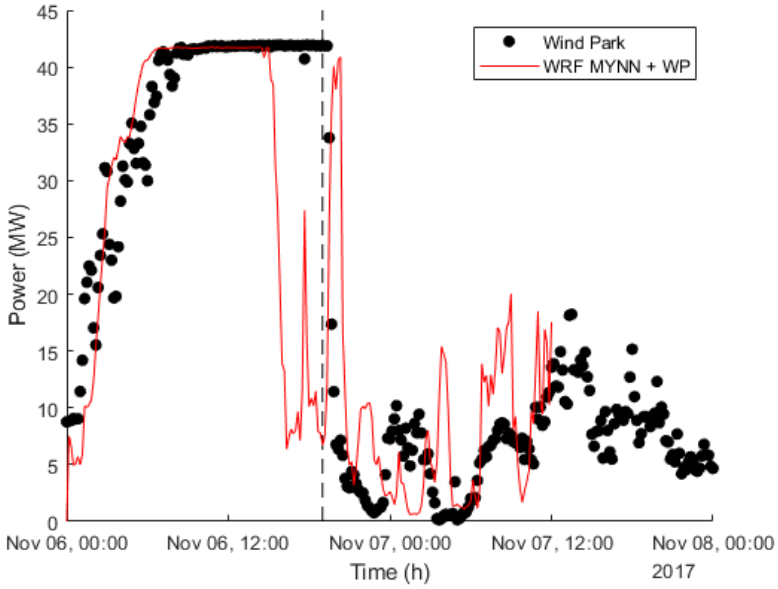

Figure 4.9: Generated power simulated by WRF (MYNN + WP).

In figure 4.9, the simulated power by WRF and the generated power from the wind farm at Edinbane is shown. As a result of the wind ramp being simulated too early (see figure 4.8), the generated power is wrongly simulated as well at this time.

Table 4.1: RMSE and NRMSE of wind speeds from simulations at the location of windfarm Edinbane

	RMSE [m s^{-1}]		NRMSE [-]	
simulation	surface	hub height	surface	hub height
YSU	8.5184	4.6338	0.4483	0.4251
MYNN2.5	8.7815	4.6456	0.4622	0.4262
MYNN2.5 + WF	8.6193	4.6105	0.4536	0.4230

In table 4.1, the RMSE (equation 4.1) and the normalised RMSE (equation 4.2) for the WRF simulations over Edinbane with different PBL schemes are given. The RMSE at the surface is normalised with the weather station observations, the RMSE at hub height is normalised with the wind park observations. The RMSE is smaller for the wind speed at hub height than for the wind speed at the surface. The difference between the performance of the different PBL schemes is not very large. For the wind speed at the surface, the YSU seems to give the best results, but the difference with the other PBL schemes is small. At hub height, all PBL perform comparably.

In figure 4.10, similar plots are shown for Aberdeen. Here, the observations from the LiDARs are included as well. All observations and the model output show an increase in wind speed over more than 24 hours. Around 0700 UTC, November 7, the wind speed suddenly drops. The offshore LiDAR and the weather station show this ramp down to be around 0700 UTC. Unfortunately no data from the onshore LiDAR is available. For the wind speed at the surface (figure 4.10a), the WRF with YSU scheme models a higher wind speed before the the passing of the cold front and a very sudden ramp down after its passing. The WRF-MYNN2.5 (both with and without wind farm parametrisation) are very similar and show a gradual increase in wind speed before the passing of the cold front. After its passing, there is a decrease in wind speed but it is not as steep as the WRF-YSU output and the offshore LiDAR observations. At hub height, the same general pattern can be seen; an increase in wind speed as the cold front approaches and a sudden drop in wind speed once it passes. The ramp down shown by WRF-MYNN2.5 (with and without wind farm parametrisation) is a lot steeper than at the surface, but still less drastic as shown by WRF-YSU. Appendix D, F, E and G show that in general the wind speed is higher in the YSU output.

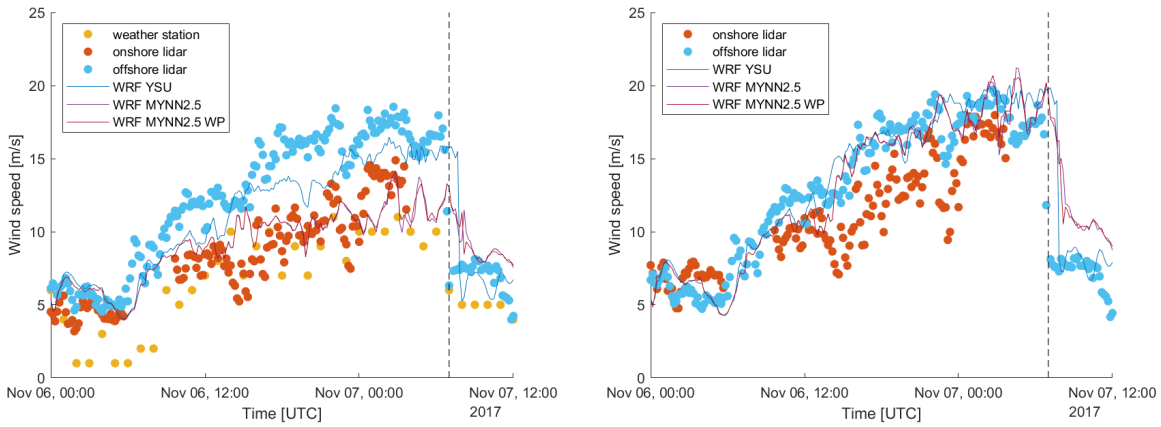

(a) Surface height (10m).

(b) Hub height (64m).

Figure 4.10: Wind speed measurements and WRF output at the location of the offshore LiDAR in Aberdeen.

In table 4.2, the RMSE (equation 4.1) and the normalised RMSE (equation 4.2) for the WRF simulations over Aberdeen with different PBL schemes are given. The RMSE at the surface is normalised with the weather station observations, the RMSE at hub height is normalised with the LiDAR observations. Again, the RMSE is smaller at hub height than at the surface. For the wind speed at the surface, the YSU clearly gives the worst results. However, at hub height the YSU gives the best results.

In figure 4.11, the WRF simulations and the wind profiler observations over South Uist are shown. When the upper winds decrease around 1900 UTC, the wind speed simulated by WRF seems to increase. In figure 4.12, the same is shown for Aberdeen, and the LiDAR measurement are included. The LiDAR measurements and the wind profiler measurements differ substantially at lower heights. The WRF simulations seem to cor-

Table 4.2: RMSE and NRMSE of wind speeds from simulations at the location of the offshore LiDAR in Aberdeen.

	RMSE [m s^{-1}]		NRMSE [-]	
simulation	surface	hub height	surface	hub height
YSU	7.5870	2.2440	0.8430	0.1444
MYNN2.5	5.6530	2.4370	0.6281	0.1568
MYNN2.5 + WF	5.5903	2.4150	0.6211	0.1554

respond best with the wind profiler observations in the lowest 500 meters, but differ above that. Once the FLLJ has passed, the correspondence with both the wind profiler and the LiDAR observations improves.

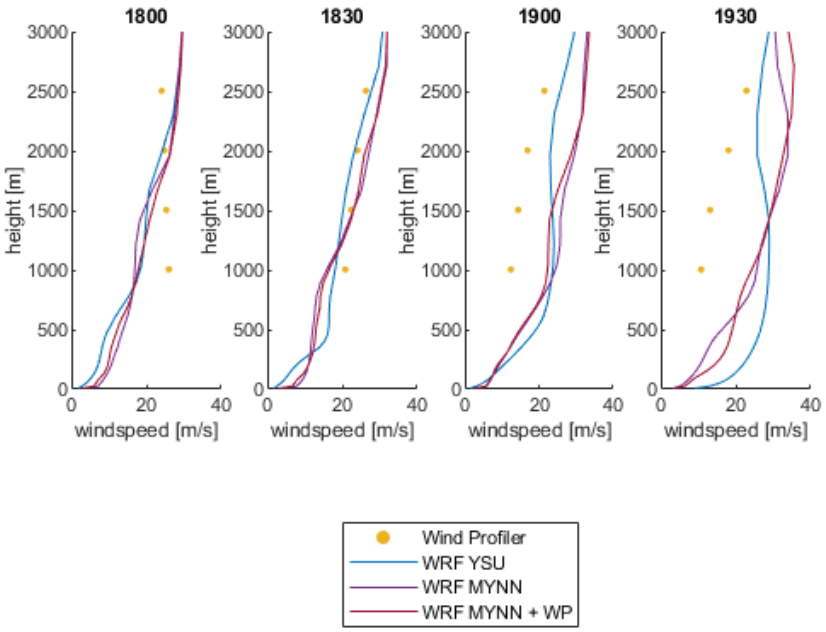

Figure 4.11: Wind profiler measurements and WRF simulations at South Uist on November 6.

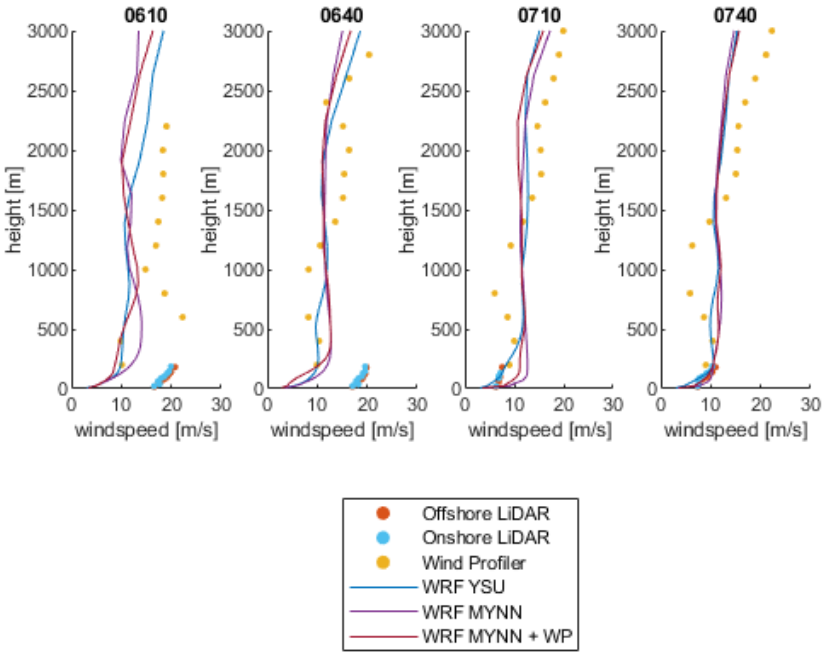

Figure 4.12: Wind profiler measurements over Hill of Dudwick, offshore LiDAR measurements and WRF simulations over Aberdeen on November 7.

In figure 4.13 the time-height plot of the wind speed is visible for the different WRF runs. The YSU simulation shows the development of a FLLJ around 0600 UTC on the 6th of November. The FLLJ persists until it collapses around 1600 UTC on the 6th. However, a couple of hours later an FLLJ forms again, seemingly reaching the same wind speeds and depth as during the first FLLJ. The lowest layer seems off compared to the rest of the image. The MYNN2.5 simulation roughly shows the same pattern, but the gap between the two LLJs is larger here. The same goes for the MYNN2.5 + WP simulation.

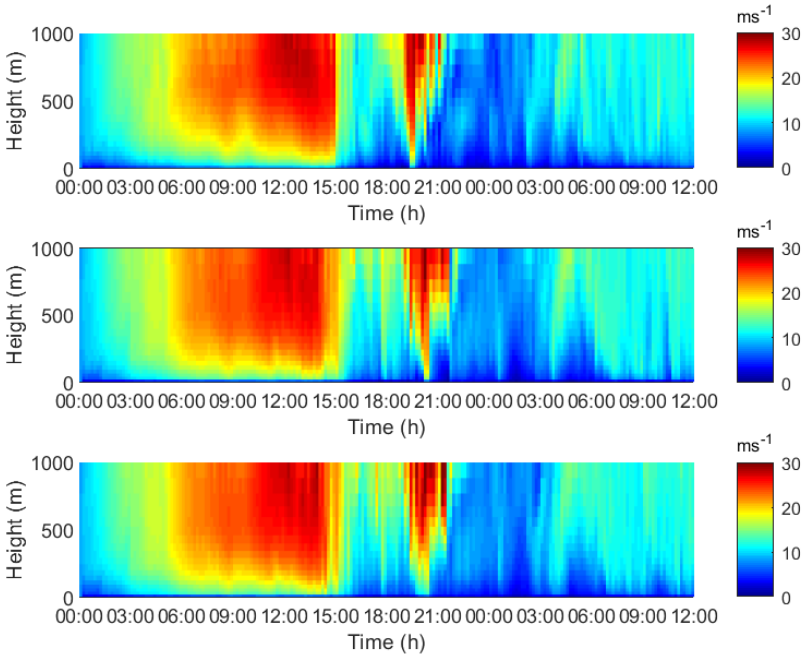

Figure 4.13: Time-height plots of wind speed at the location of windfarm Edinbane on November 6 for YSU, MYNN and MYNN + WP, respectively.

In figure 4.14 similar plots are shown for the WRF output over Aberdeen. Also the observations from the floating LiDAR are added. All of the WRF plots show a similar pattern: an FLLJ develops around 1200 UTC at November 6, persists throughout the night and quickly dissolves around 0700 UTC at November 7. The LiDAR observations confirm this pattern, be it only for the lowest 200 meters.

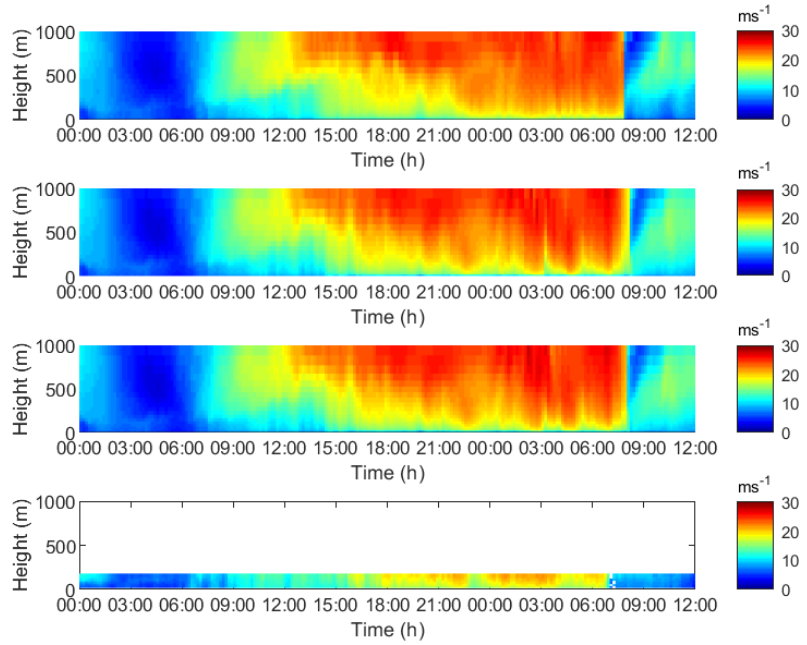

Figure 4.14: Time-height plots of wind speed over Aberdeen on November 6th and 7th for YSU, MYNN, MYNN + WP and the offshore LiDAR, respectively.

4.5.1. ERA5

By the end of this research, it was possible to run WRF with ERA5 instead of ERA-Interim. Using WRF with ERA5 could potentially lead to better results. ERA5 has a higher spatial resolution and more pressure levels than ERA-Interim. With hourly analysis fields instead of 6-hourly, the temporal resolution is also higher. These improvements in resolution could lead to better results in the WRF simulation [Hennermann and Guillory, 2019]. Figures 4.15a, 4.15b, 4.15c and 4.15d show the result of a simulation using ERA5 and the MYNN2.5 PBL scheme with wind farm parametrisation. Most notable is that in this simulation the wind ramp is simulated at the same time as the observations show at Edinbane. At Aberdeen, the differences with the ERA-Interim simulations are smaller. However, the simulated wind speed at hub height at Aberdeen has several peaks compared tot the LiDAR observations. Figure 4.16 shows the simulated power for the wind farm at Edinbane. As a result of the wind speed being simulated better compared to the ERA-Interim runs, the power simulations of the ERA5 runs also improve.

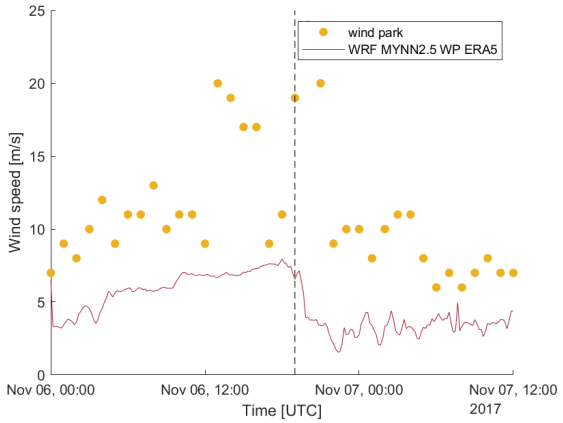

(a) Measurements and WRF simulations of wind speed at surface height (10m) at Edinbane.

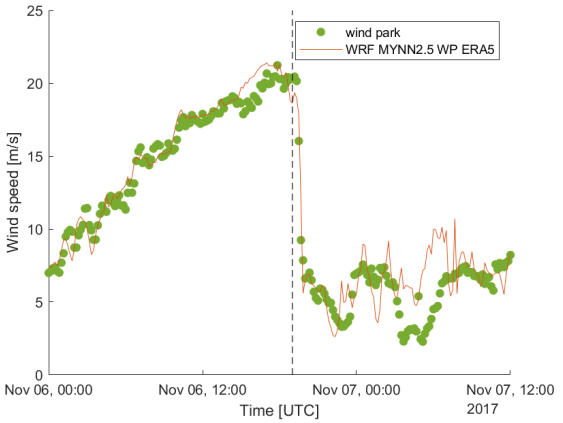

(b) Measurements and WRF simulations of wind speed at hub height (64m) at Edinbane.

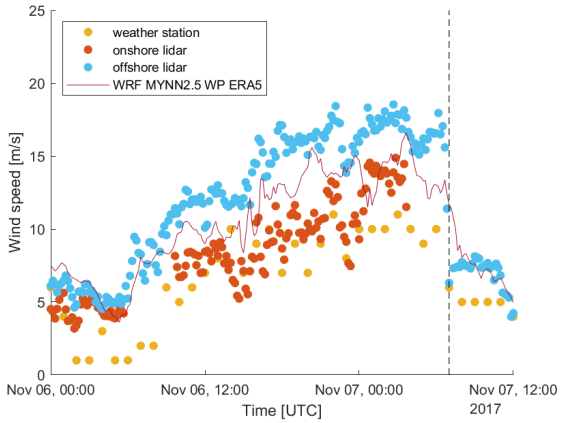

(c) Measurements and WRF simulations of wind speed at surface height (10m) at Aberdeen.

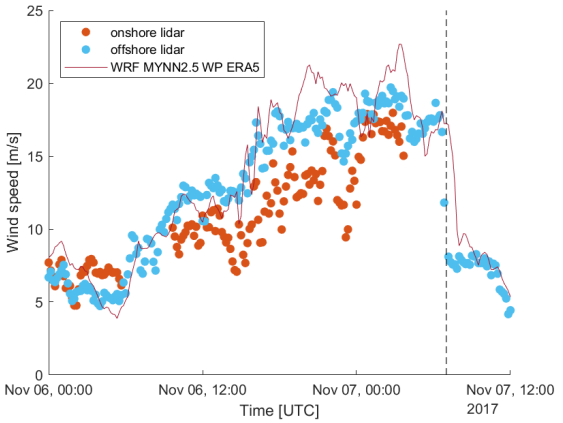

(d) Measurements and WRF simulations of wind speed at hub height (64m) at Aberdeen.

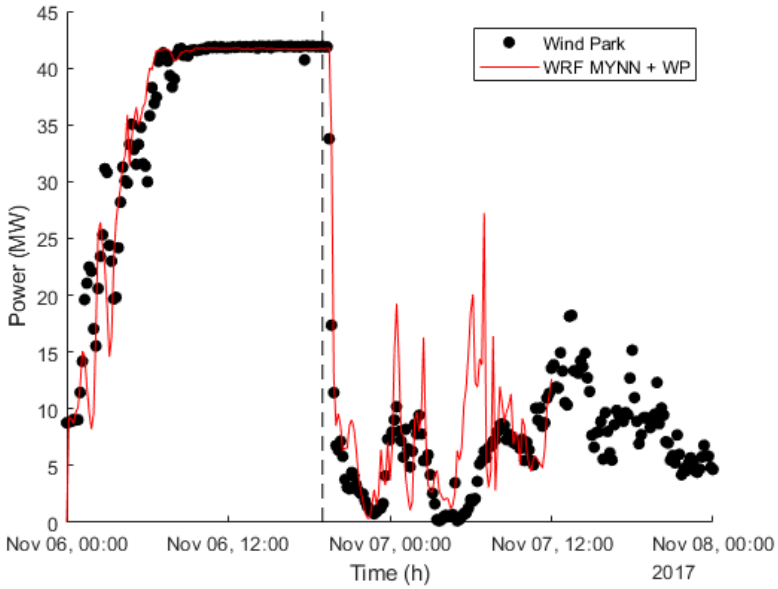

Figure 4.16: Generated power simulated by WRF (MYNN + WP).

5

Case Study II

The second case study that will be evaluated is the passing of a cold front over Scotland during the 16th of November, 2017.

5.1. Synoptic Situation

On the 16th of November, there was a strong low pressure system east of Iceland. A warm pressure area is located west of Ireland. As can be seen in figure 5.1a, a cold front passed over Edinbane around 0000 UTC. This cold front passed over Aberdeen around 0600 UTC (see figure 5.1b).

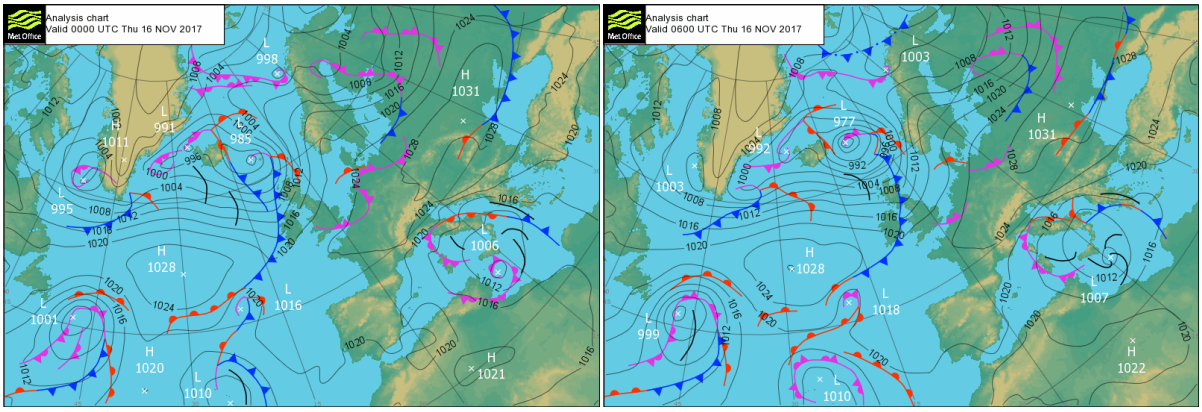

(a) Synoptic map of 0000 UTC, November 16, 2017 [MetOffice, 2017b].

(b) Synoptic map of 0600 UTC, November 16, 2017 [MetOffice, 2017b].

Figure 5.1: Synoptic maps for Case Study II.

5.2. Satellite Observations

In figure 5.2, a satellite image from Europe on November 16, 0600 UTC is shown. This image shows the band of clouds layer over Ireland and the Northern part of the United Kingdom. When comparing this with figure 5.1b, the band of clouds corresponds with the location of the cold front at this time.

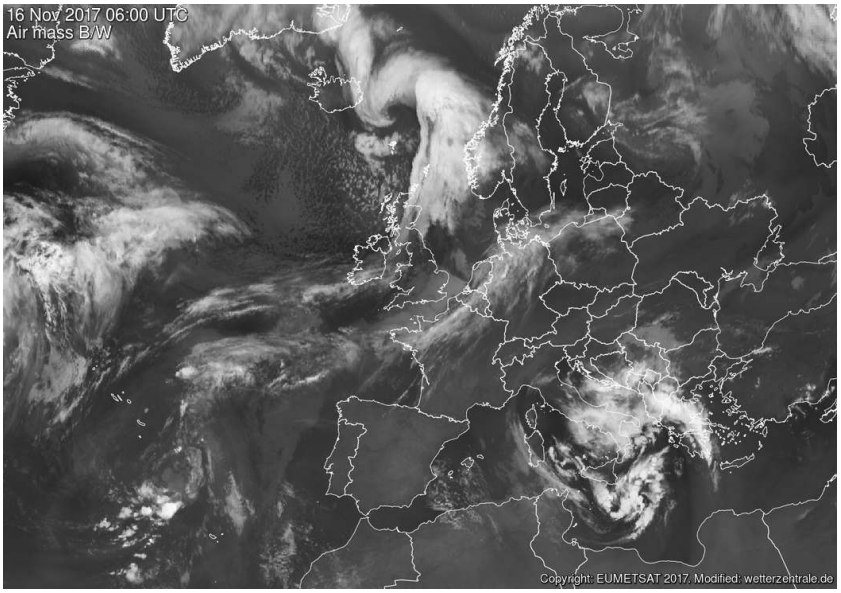

Figure 5.2: Satellite image of airmass over Europe on November 7.

5.3. SURFACE OBSERVATIONS

The measurements shown in figure 5.3a from weather station Bealach Na Ba also show the passing of a cold front around 1900 UTC. The passing of the cold front is again clearly visible in the data from weather station Dyce (see figure 5.3b). In figure 5.3c the means sea level pressure for Aberdeen is plotted. This also shows a sudden change in trend in the pressure when the cold front passes. Unfortunately, no pressure data from Edinbane is available.

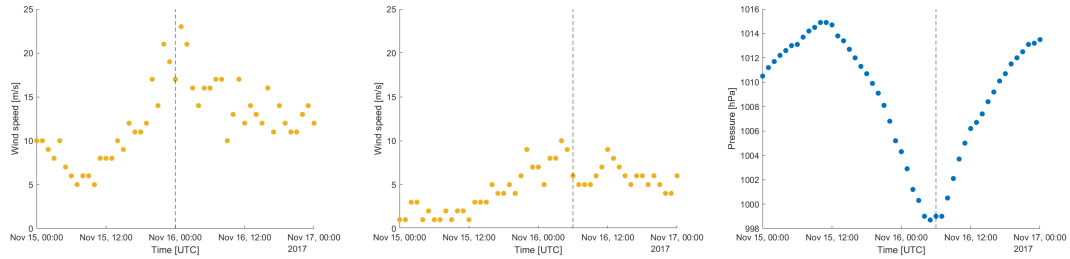

(a) Wind speed measurements at Edinbane. (b) Wind speed measurements at Aberdeen. (c) Mean sea level pressure at Aberdeen.

Figure 5.3: Surface measurements from MetOffice weather stations.

5.4. UPPER AIR OBSERVATIONS

The data from wind farm Edinbane also shows the passing of the cold front. The wind speed measurements at hub height in figure 5.4a show a drop in wind speed after the cold front passes. Logically, this leads to a drop in power production at the wind farm (see figure 5.4b). As in the other case study, it should be noted that the wind speed at the surface at Edinbane (figure 5.4a) is as high or sometimes even higher as the wind speed at hub height (figure 5.5).

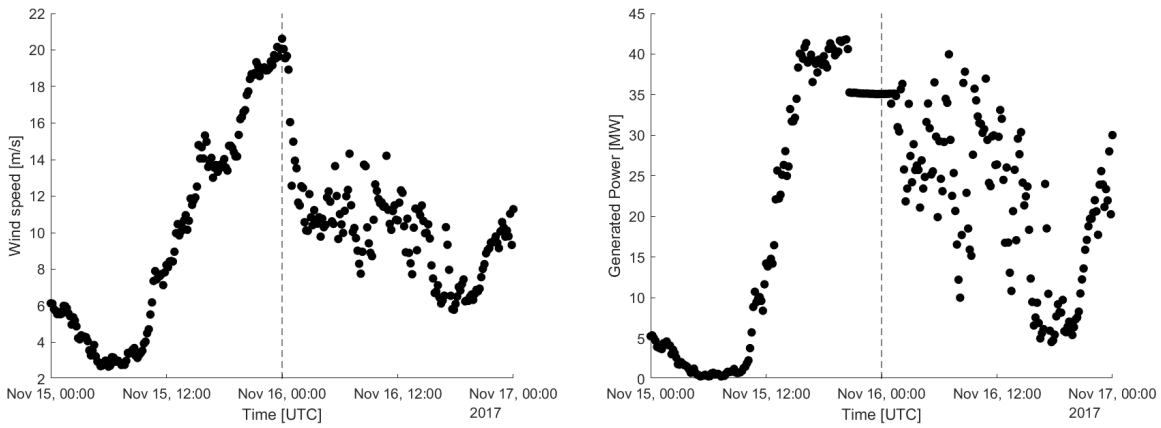

(a) Wind speed at hub height at wind farm Edinbane.

(b) Generated power at wind farm Edinbane.

Figure 5.4: Measurements at hub height at wind farm Edinbane.

The measurements from the wind profiler at South Uist start around a 1000 meters and go up till 15 kilometres. As can be seen in figure 5.5, the wind speed at an altitude of 1000 meters drops from 32 [m s^{-1}] to 15 [m s^{-1}] in a little over an hour. After 0030 UTC, no data is available.

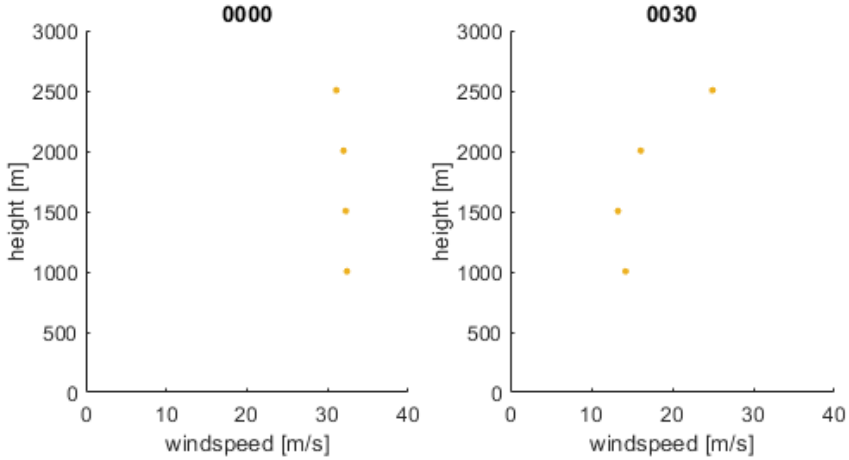

Figure 5.5: Wind profiler measurements over Hill of Dudwick and on November 16

Figure 5.6 shows the LiDAR and wind profiler observations around the time the cold front passes over Aberdeen. Especially the LiDAR observations show a fast decrease in wind speed within an hour.

From the LiDAR observations, a time-height plot could be made (see figure 5.7). This image shows the development of an FLLJ around 2000 UTC at November 15. This FLLJ seems to persist until 1300 UTC the next day, although there are some fluctuation in wind speed in these lowest 200 meters.

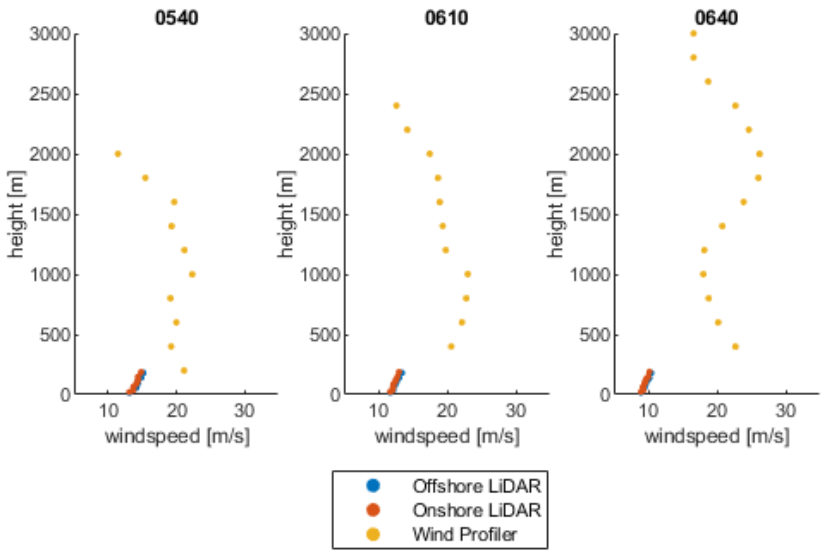

Figure 5.6: Wind profiler measurements over Hill of Dudwick and LiDAR measurements over Aberdeen on November 16

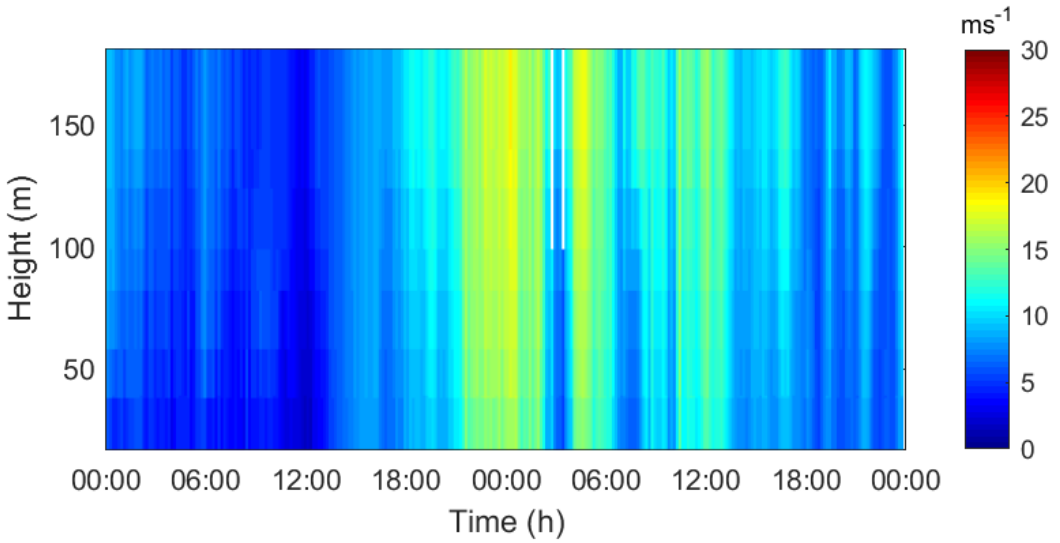

Figure 5.7: Offshore LiDAR observations from 0000 UTC, November 15 till 0000 UTC, November 17, at Aberdeen.

5.5. MESOSCALE MODELLING

In figure 5.8 the observed and modelled wind speed over Edinbane at the surface (5.8a) and at hub height (5.8b) are plotted. The observations from the weather station show an increase in wind speed when the cold

Table 5.1: RMSE and NRMSE of wind speeds from simulations at the location of wind farm Edinbane

	RMSE [m s^{-1}]		NRMSE [-]	
simulation	surface	hub height	surface	hub height
YSU	7.8067	2.9195	0.4109	0.2950
MYNN2.5	8.5291	3.3078	0.4489	0.3342
MYNN2.5 + WF	8.4248	3.3483	0.4434	0.3383

front is approaching and a decrease once the cold front has passed. This pattern is also visible in output from the WRF simulations, although the wind speed after the cold front has passed is much lower than what is observed by the weather station. When comparing the model output at hub height to the wind speed measured at this height by the wind turbines, the wind speed from the WRF simulations roughly agrees with the observations before then cold front passes, but starts fluctuating a lot once the cold front passed.

In table 5.1, the RMSE (equation 4.1) amd the NRMSE (equation 4.2) for the different WRF runs over Edinbane can be found. Like in the first case study, all models perform better at hub height than at the surface. The YSU simulation peforms best, both at the surface and at hub height.

In appendix H, J and L the surface wind speed maps for the YSU, MYNN2.5 and MYNN2.5 + WF runs can be found. All these maps show band of strong winds laying just Northwest of Scotland at 12PM, November 15.

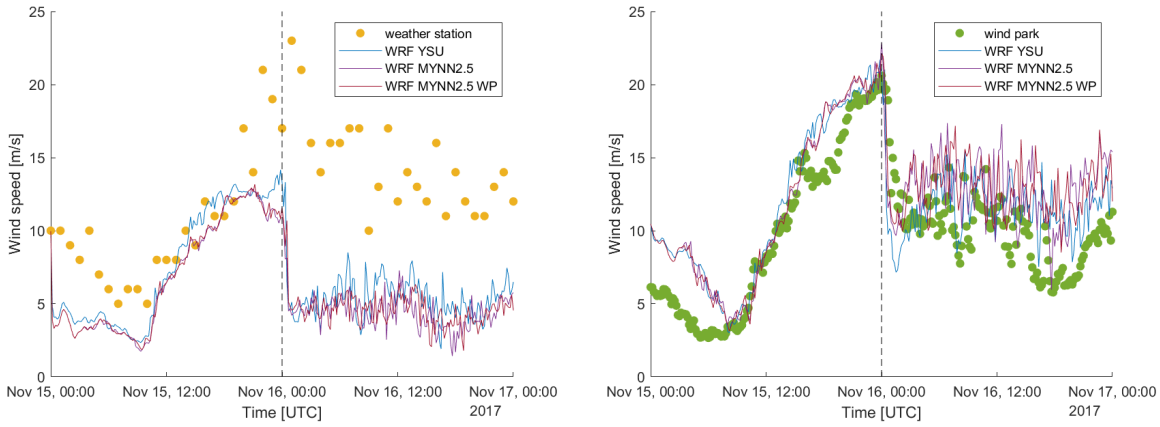

(a) Surface height (10m).

(b) Hub height (64m).

Figure 5.8: Wind speed measurements and WRF output at the location of wind farm Edinbane

In figure 5.9a and figure 5.9b, plots can be found for Aberdeen. Here, the passing of the cold front is less noticeable. The wind speed measured by the weather station is increasing and seems to stabilize once the cold front passed, but there is not a clear decrease. The data from the LiDAR is fluctuating a lot and does not show a clear pattern. The output data from WRF shows a sudden decrease in wind speed just when the cold front passes, but increases quickly again after its passing.

In table 5.2, the RMSE(equation 4.1) amd the NRMSE (equation 4.2) for the different WRF runs over Aberdeen can be found. Like in the first case study, all models perform better at hub height than at the surface. The difference between the different PBL schemes is small at both heights. At the surface, the MYNN2.5 + WF peforms best and at hub height, the YSU simulation gives the best results.

In figures 5.10, the simulated power by WRF and the generated power from the wind farm at Edinbane is shown. The formation of the FLLJ is modelled relatively well. The generated power at the wind farm has a strange pattern just before the cold front passes, so this data could be faulty. After the passing of the front, both the data from the wind farm and the simulation show very widespread values.

The surface wind speed maps for all different WRF simulations can be found in appendix H, J and L. These maps all show a band of higher winds laying just of the coast of Aberdeen. As in the first case study, the structure of the FLLJ is very distinctive. Just before the cold front, the wind direction is parallel to the front. After the front passes, the wind veers to a wind direction perpendicular to the front. The passing of the front corresponds with a dip in temperature of a couple degrees.

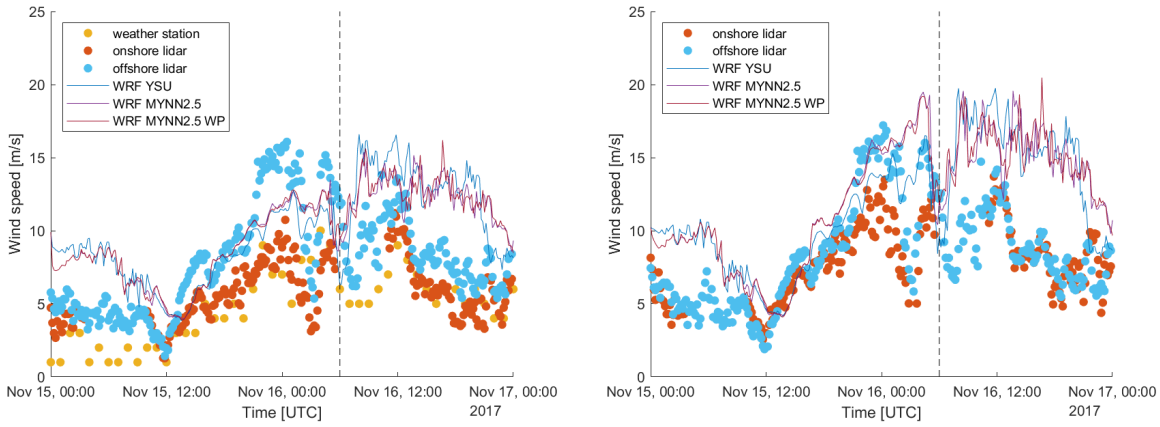

(a) Surface height (10m).

(b) Hub height (64m).

Figure 5.9: Wind speed measurements and WRF output at the location of the offshore LiDAR in Aberdeen.

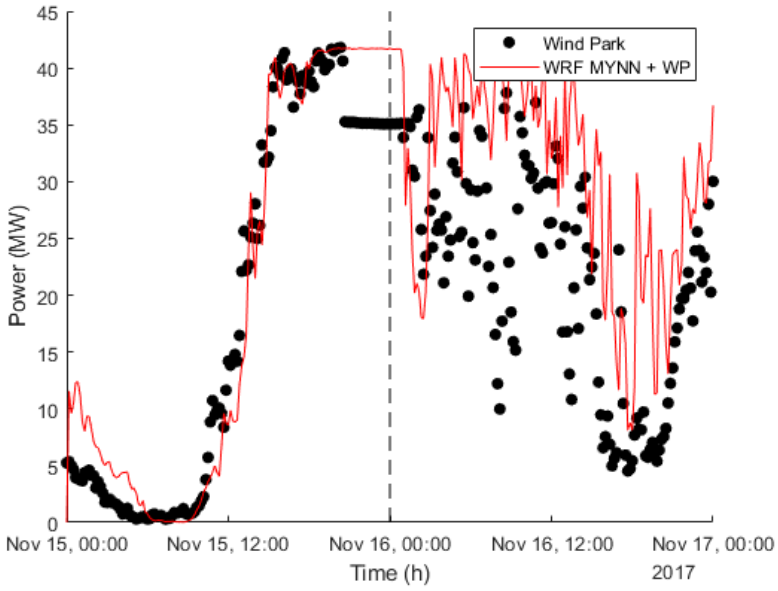

Figure 5.10: Generated power simulated by WRF (MYNN + WP).

Table 5.2: RMSE and NRMSE of wind speeds from simulations at the location of the offshore LiDAR in Aberdeen.

	RMSE [m s^{-1}]		NRMSE [-]	
simulation	surface	hub height	surface	hub height
YSU	6.0393	4.8413	0.6710	0.3162
MYNN2.5	5.8579	4.9651	0.6509	0.3243
MYNN2.5 + WF	5.7097	4.9365	0.6344	0.3225

In figure 5.11, the vertical profiles of the WRF simulations for wind speed are compared with the observations of the wind profiler over South Uist. The vertical profile at 0000 UTC is largely simulated correctly by all of the different set-ups. The ramp down is simulated above a 1000 meters by the different set-ups but does differ a bit from the observations. Below a 1000 meters, there are no observations to compare the simulations with. In figure 5.12, the vertical profiles of the WRF simulation are shown, together with the wind profiler and the LiDAR observations over Aberdeen are shown. At 0540 UTC, the simulations correspond well with the observations. When the ramp down occurs, the simulations seem to miss this or simulate it later.

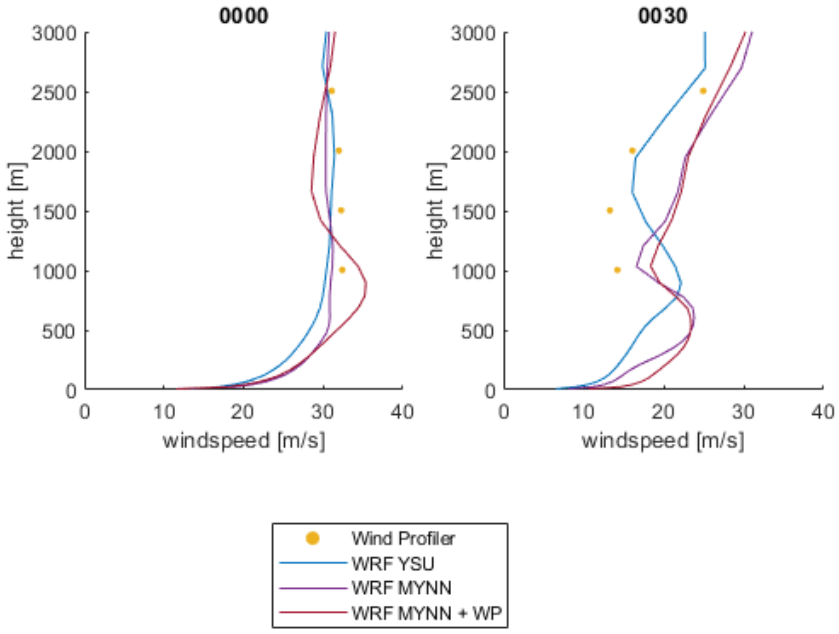

Figure 5.11: Wind profiler measurements over Hill of Dudwick and WRF simulations over South Uist on November 16.

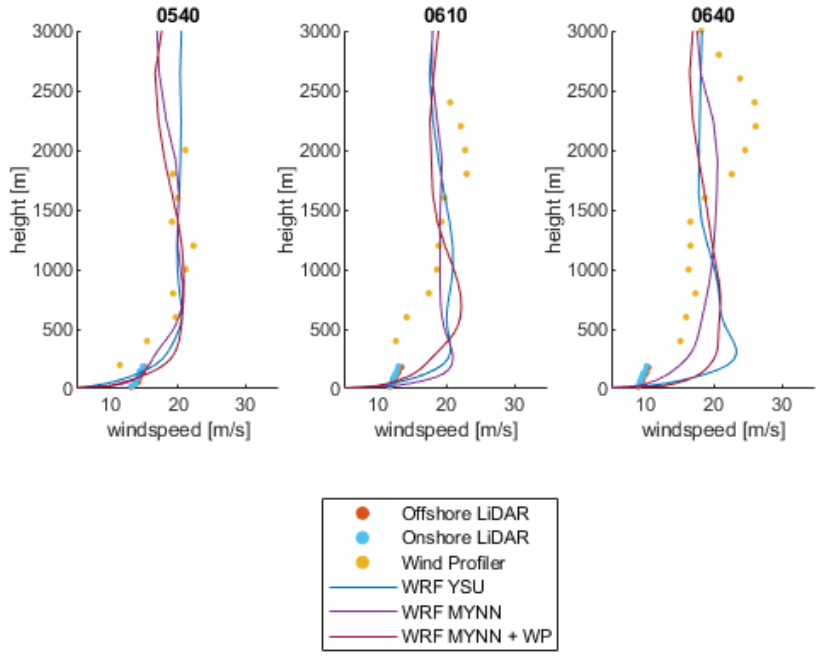

Figure 5.12: Wind profiler measurements over Hill of Dudwick, offshore LiDAR measurements and WRF simulations over Aberdeen on November 16.

In figure 5.13, time height plots for all different PBL schemes are shown. All of these show the development of an FLLJ around 1400 UTC, which persists through the night and quickly dissolves just after midnight.

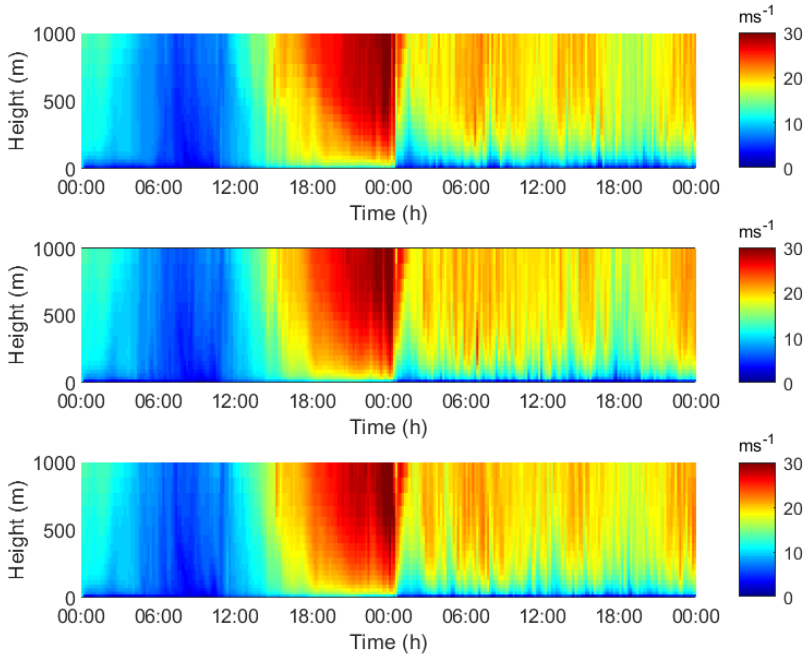

Figure 5.13: Time-height plots of wind speed at wind farm Edinbane on November 6 for YSU, MYNN and MYNN + WP, respectively.

In figure 5.14 similar plots for Aberdeen are shown. An FLLJ develops around 1200 PM, November 15, and quickly dissolves around 0600 AM, November 16. After the FLLJ dissolves, some peaks in wind speed occur.

In the plots for the MYNN2.5 scheme, these peaks are more intense and frequent. The wind speed observed by the LiDAR seems a bit lower than the modelled with speeds but the general pattern corresponds.

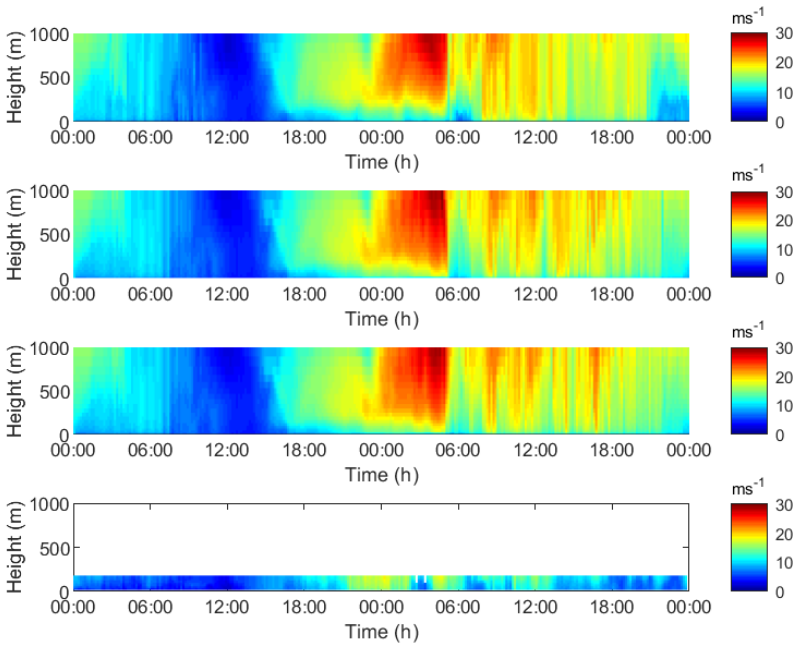

Figure 5.14: Time-height plots of wind speed at Aberdeen on November 16 for YSU, MYNN, MYNN + WP and the offshore LiDAR, respectively.

6

CONCLUSIONS & RECOMMENDATIONS

Several datasets with observational data have been used to determine case studies of FLLJs. Once the case studies were determined, WRF runs were performed over these cases.

6.1. DISCUSSION

The measurements from the weather station at Edinbane seem to be a bit off compared to the observations at hub height and the WRF simulations. Like mentioned in chapter 3, the weather station is located on the edge of a cliff. This could have an influence on the wind speed measurements of this station.

The measurement from the onshore and offshore LiDAR do differ in the observed case studies, especially at the surface. The offshore LiDAR measures higher wind speeds in general. This could be explained by the higher wind speeds at sea, but difference in wind speeds between the LiDARs is quite high considering the distance between the two LiDARs is only a few kilometres. Unfortunately, there were some gaps in the data from the LiDARs. A measurement campaign with multiple LiDARs measuring simultaneously with some distance between them can be very valuable for studying the development of wind profiles over time and distance. However, the reliability of the measurement instruments has to be very good in order to use the measurements for research.

6.2. CONCLUSIONS

This thesis was started with the following questions:

1. What are the characteristics of the wind fields associated with FLLJs?
2. Can FLLJs be simulated reliably and how does this depend on PBL schemes?

Based on the observations by the weather stations, the wind profilers and the lidars, the following characteristics of a FLLJ can be identified; once a FLLJ forms, it persists for several hours. Within the FLLJ, the wind direction is parallel to the cold front. After the front passes wind direction veers until it is perpendicular to the cold front. After the front passes, the temperature drops a couple degrees. The wind speed increases during the occurrence of the FLLJ, and drops very suddenly after the front passes; a ramp down occurs. The observed ramp downs following the FLLJ agree with the observations of Browning and Pardoe [1973].

WRF simulations simulate FLLJs relatively well. In both case studies there was a clear difference in performance between the wind speed simulation at the surface and at hub height. The wind speed at hub height was simulated in better correspondence with the observations at both locations in both case studies. In the observed case studies, usually the development of the FLLJ was simulated in accordance with the observations. However, the collapse of the FLLJ was not simulated at the observed time in both of the case studies.

In the first case study, there was also a difference in performance of the simulation between Edinbane and Aberdeen. At Edinbane, the ramp down was simulated hours before it actually occurred. Later, the wind speed increased again to pre-ramp down wind speeds. However, this can be attributed to WRF simulating the cold front moving back and forth. At Aberdeen, the general pattern of the ramp down by the simulation agreed with the observations. The ramp down was simulated just after the observations showed it, but the absolute wind speed was off compared to the observations.

In the second case study, again there was a difference in the performance of the models at surface height and at hub height. At Edinbane, the simulations performed a lot better at hub height than for the first case study. The ramp down was simulated at the same time as the observations show it to take place. At Aberdeen, the ramp down is not very clear in the observational data. The simulations do quite well during the development of the LLJ and the approaching of the cold front. Around the passing of the cold front, the simulated wind speed drops, but peaks again soon after.

From these two case studies, it can be concluded that the simulations give reasonable results for the occurrences of FLLJs. Parts of its development and the coinciding ramp down are simulated correctly, but important developments are missing and the simulated absolute wind values often disagree with the observations. There does not seem to be a big difference between the different PBL schemes which were used. Depending on the date, location and height, one PBL schemes perform better or worse than the others, but the differences are small.

6.3. RECOMMENDATIONS

Although FLLJs do not seem to occur very frequently, they do have a noticeable effect on the amount of energy that is generated by a wind farm. Therefore, it is a phenomena that should be taken into account for wind energy forecasts. Predicting the ramp down after the passing of a FLLJ leads to knowing whether the amount of energy produced by other sources should be adapted.

Another thing that can be taken from this research is the disability of WRF to properly simulate FLLJs. Further research into why this is the case and whether it can be solved could be beneficial for the general accuracy of the WRF model. An option would be to test other, more complex PBL schemes. The PBL schemes used in this research lead to similar results, but also perform differently at some times and locations. Further research into why these schemes lead to other results might be beneficial to decide on which PBL scheme to use. Another option would be to see whether a double-moment microphysics scheme would improve the simulations, since these schemes tend to perform better in large-scale environments.

The WRF simulations in this research were performed with ERA-Interim as the initial and boundary conditions. Because of the promising results in section 4.5.1, investigating the performance of ERA5 in cases of a FLLJ is something that should be considered in the future.

Wind turbines are still growing in size and will likely continue to do so in the future. Also the developments of AWEs results in higher altitudes being reached. Therefore, more research should be done into winds at these altitudes. The uncertainties in wind energy predictions are still one of the weak spots and any improvement in this could result in a better integration of wind turbines in the existing electricity grid.

A

Measurement Locations

B

Surroundings Weather Station Bealach Na Ba

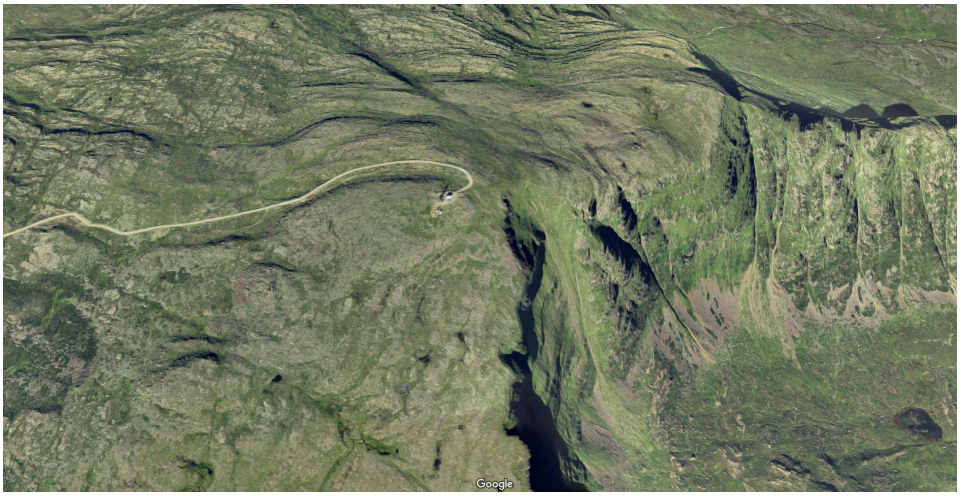

C

WRF DOMAINS

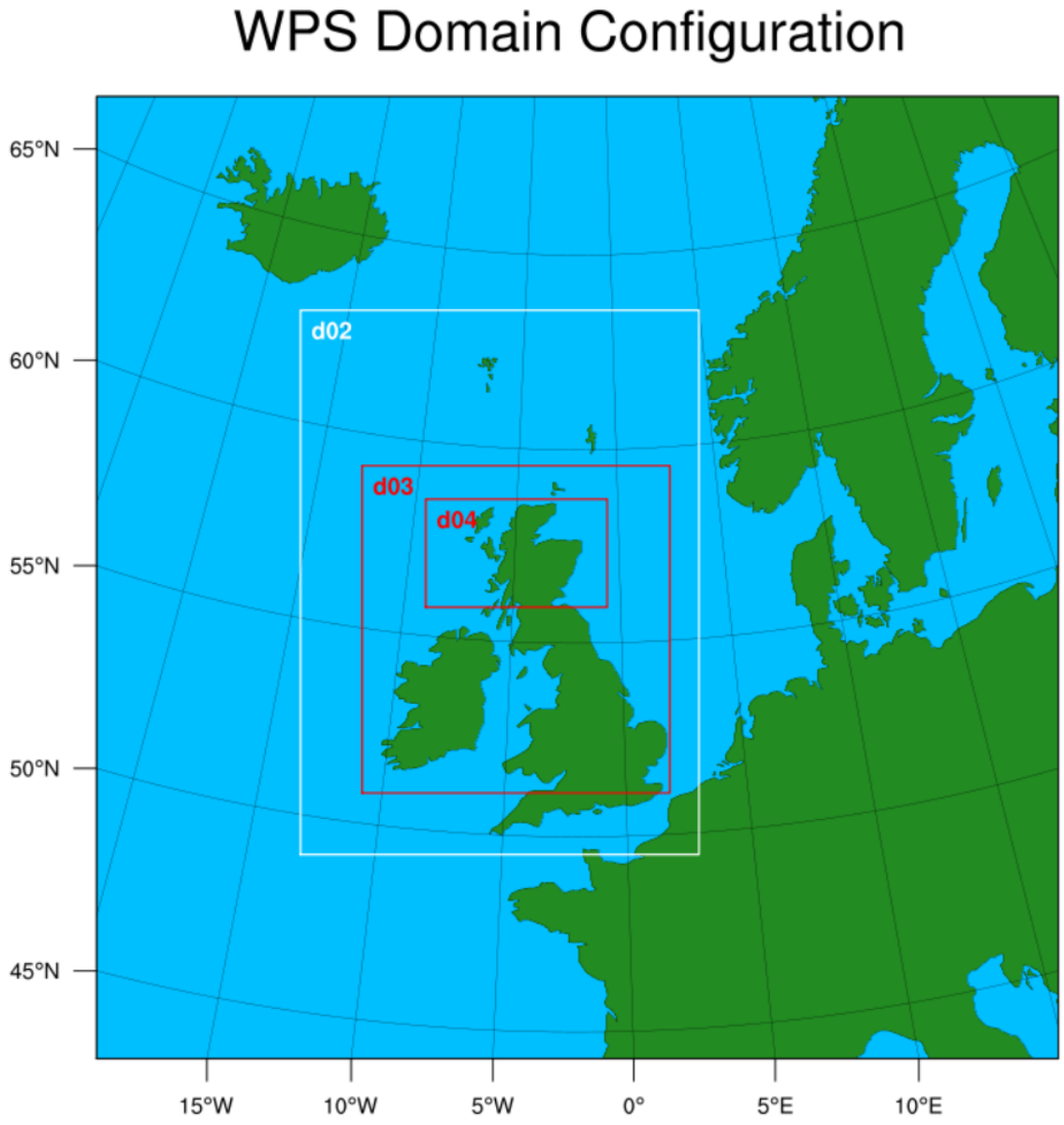

D
WIND SPEED AT SURFACE - CASE STUDY I - YSU

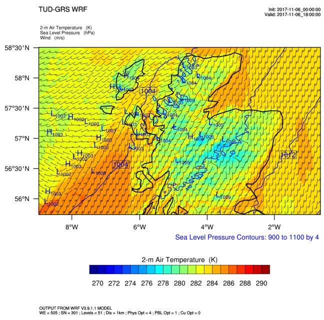

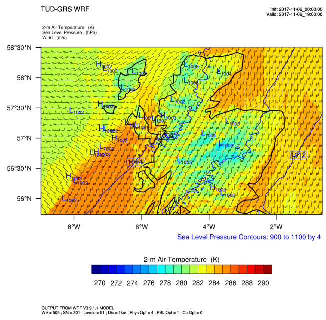

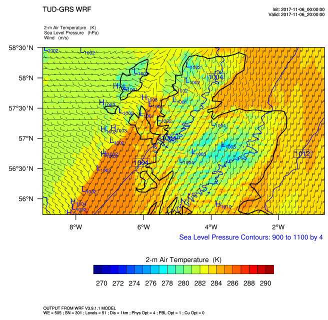

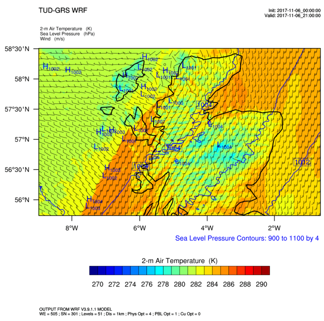

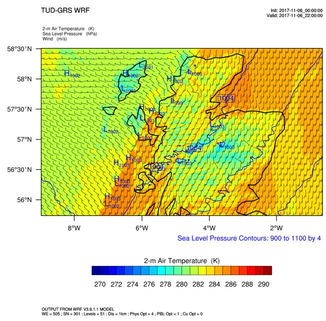

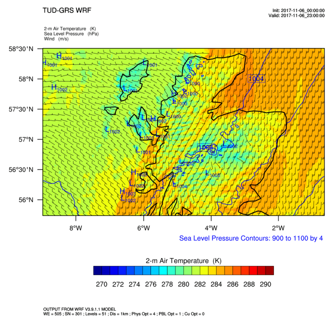

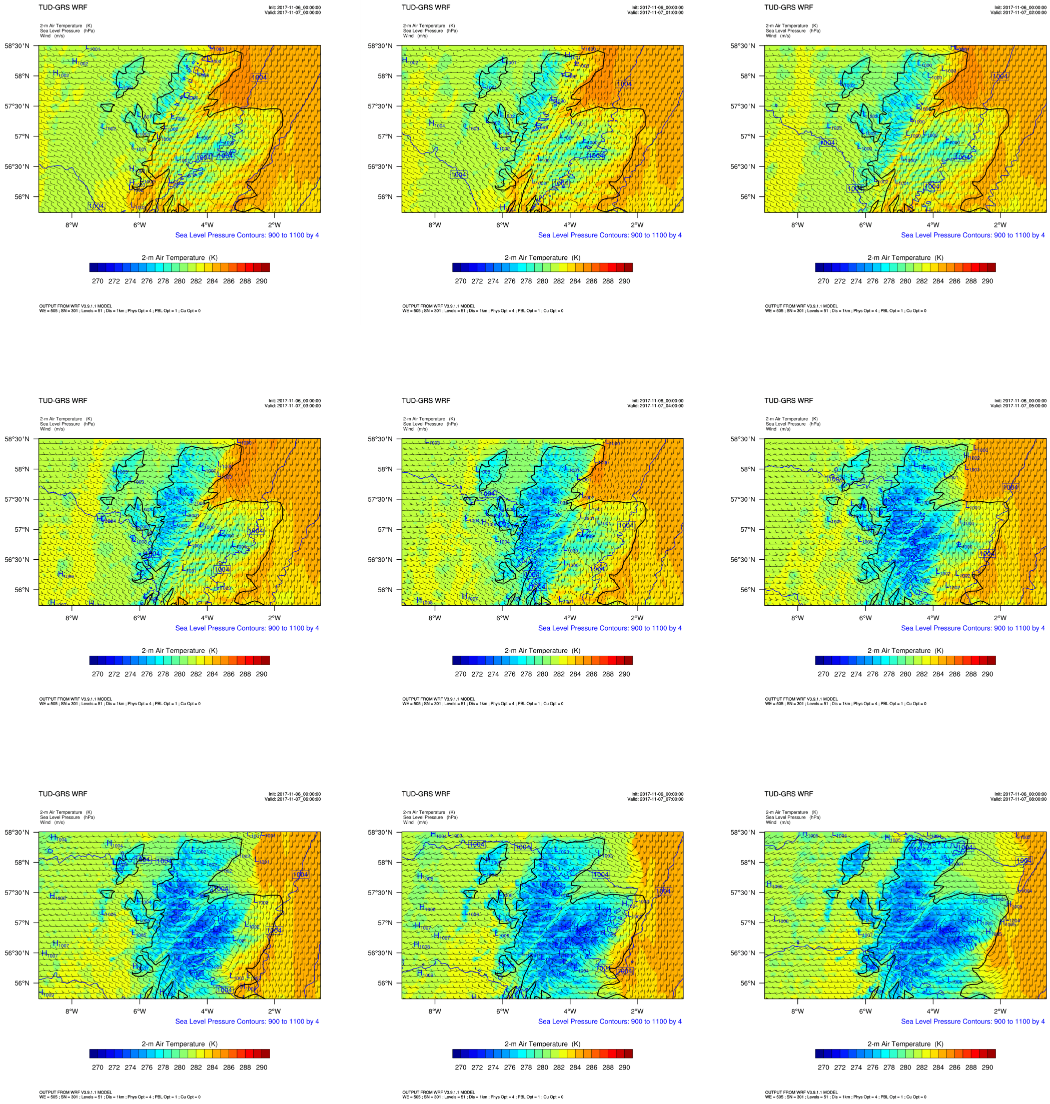
TUD-GRS WRF
2-m Air Temperature (K)
Sea Level Pressure (hPa)
Wind (m/s)
Sea Level Pressure Contours: 900 to 1100 by 4
2-m Air Temperature (K)
270 272 274 276 278 280 282 284 286 288 290
58°30'N
58°N
57°30'N
57°N
56°30'N
56°N
8°W
6°W
4°W
2°W

E

WIND SPEED AT HUB HEIGHT - CASE STUDY I - YSU

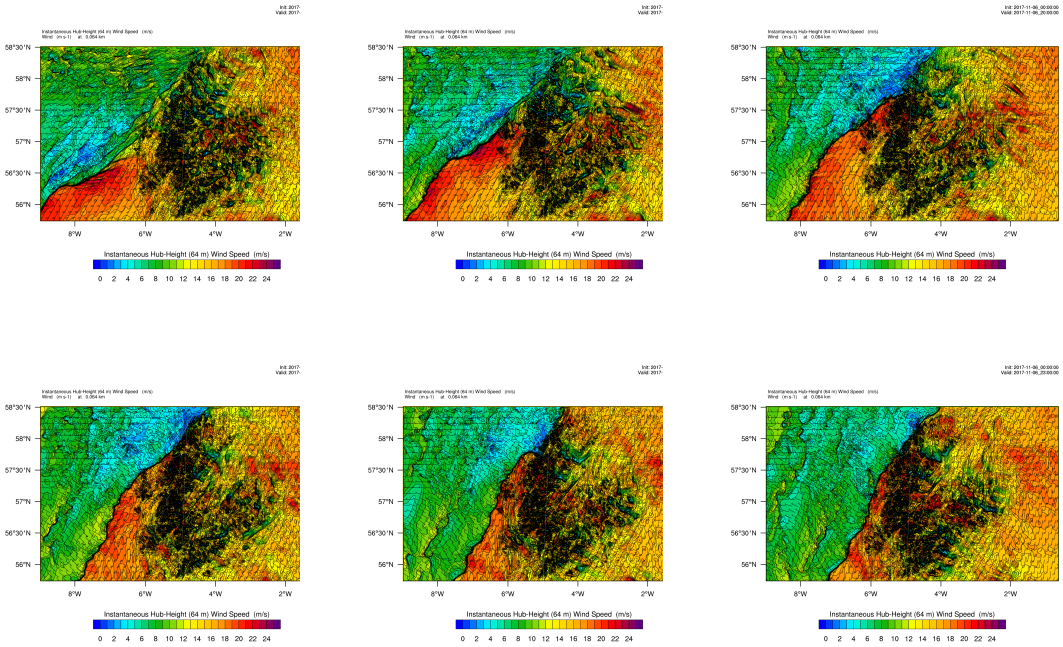

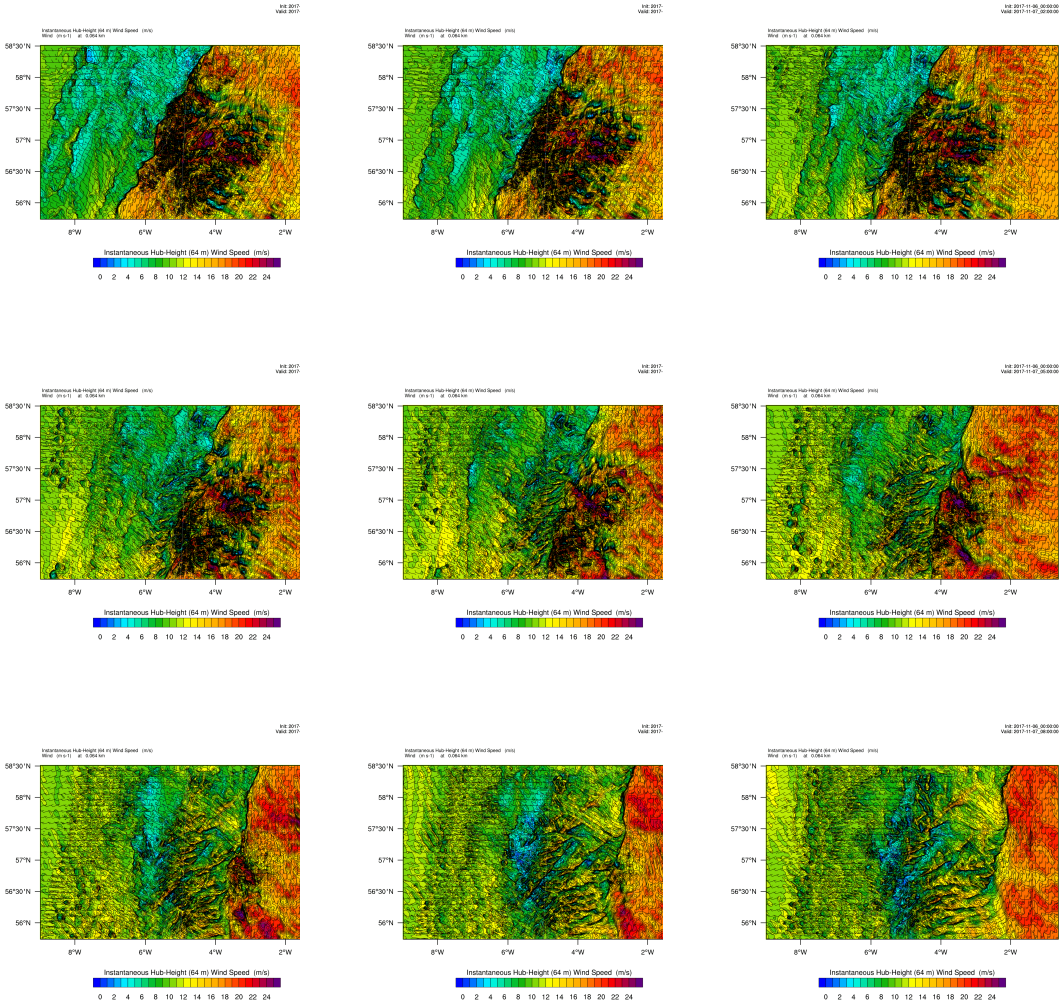
Init: 2017-
Valid: 2017-
Instantaneous Hub-Height (64 m) Wind Speed (m/s)
Wind (m s-1) at 0.064 km
58°30'N
58°N
57°30'N
57°N
56°30'N
56°N
8°W
6°W
4°W
2°W
Instantaneous Hub-Height (64 m) Wind Speed (m/s)
0 2 4 6 8 10 12 14 16 18 20 22 24
Init: 2017-11-06_00:00:00
Valid: 2017-11-07_00:00:00
Init: 2017-11-06_00:00:00
Valid: 2017-11-07_06:00:00

F

WIND SPEED AT SURFACE - CASE STUDY I - MYNNWP

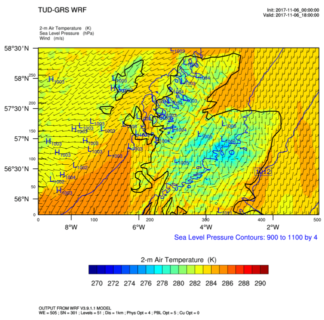

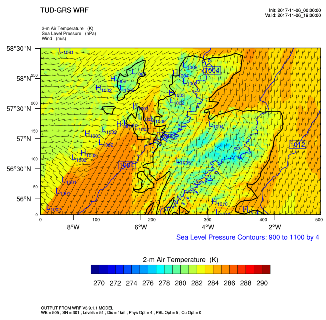

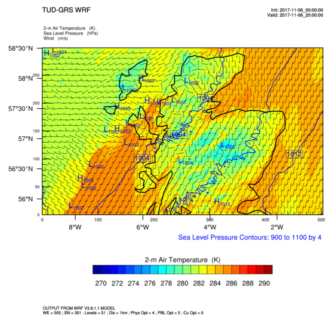

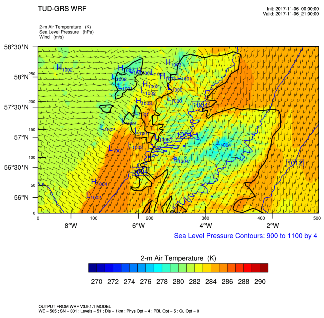

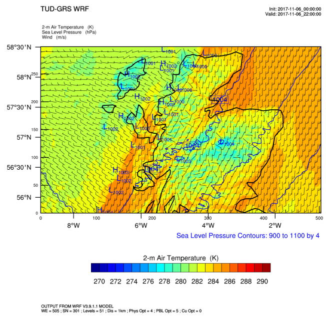

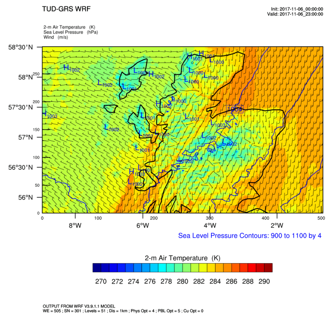

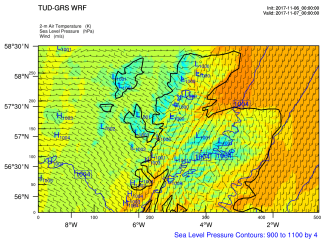
TUD-GRS WRF
Init: 2017-11-6\6_00:00:00
Valid: 2017-11-6?_30:00:00
2-m Air Temperature (K)
Sea Level Pressure (hPa)
Wind (m/s)
58°30'N
58°N
57°30'N
57°N
56°30'N
56°N
8°W
6°W
4°W
2°W
Sea Level Pressure Contours: 900 to 1100 by 4
2-m Air Temperature (K)
270 272 274 276 278 280 282 284 286 288 290
OUTPUT FROM WRF V3.9.1 MODEL
IM1 = 500 ; DM = 281 ; Levels = 51 ; Dts = 1min ; Phys Opt = 4 ; PBL Opt = 5 ; Cu Opt = 6

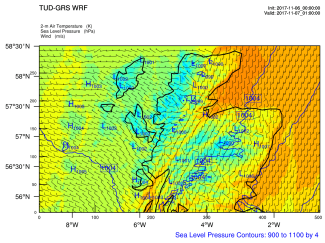
TUD-GRS WRF
Init: 2017-11-6\6_00:00:00
Valid: 2017-11-6?_31:00:00
2-m Air Temperature (K)
Sea Level Pressure (hPa)
Wind (m/s)
58°30'N
58°N
57°30'N
57°N
56°30'N
56°N
8°W
6°W
4°W
2°W
Sea Level Pressure Contours: 900 to 1100 by 4
2-m Air Temperature (K)
270 272 274 276 278 280 282 284 286 288 290
OUTPUT FROM WRF V3.9.1 MODEL
IM1 = 500 ; DM = 281 ; Levels = 51 ; Dts = 1min ; Phys Opt = 4 ; PBL Opt = 5 ; Cu Opt = 6

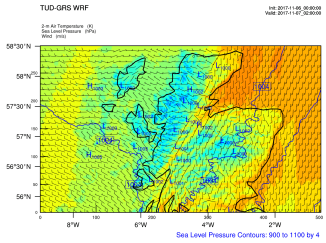
TUD-GRS WRF
Init: 2017-11-6\6_00:00:00
Valid: 2017-11-6?_32:00:00
2-m Air Temperature (K)
Sea Level Pressure (hPa)
Wind (m/s)
58°30'N
58°N
57°30'N
57°N
56°30'N
56°N
8°W
6°W
4°W
2°W
Sea Level Pressure Contours: 900 to 1100 by 4
2-m Air Temperature (K)
270 272 274 276 278 280 282 284 286 288 290
OUTPUT FROM WRF V3.9.1 MODEL
IM1 = 500 ; DM = 281 ; Levels = 51 ; Dts = 1min ; Phys Opt = 4 ; PBL Opt = 5 ; Cu Opt = 6

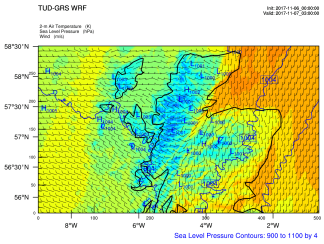
TUD-GRS WRF
Init: 2017-11-6\6_00:00:00
Valid: 2017-11-6?_33:00:00
2-m Air Temperature (K)
Sea Level Pressure (hPa)
Wind (m/s)
58°30'N
58°N
57°30'N
57°N
56°30'N
56°N
8°W
6°W
4°W
2°W
Sea Level Pressure Contours: 900 to 1100 by 4
2-m Air Temperature (K)
270 272 274 276 278 280 282 284 286 288 290
OUTPUT FROM WRF V3.9.1 MODEL
IM1 = 500 ; DM = 281 ; Levels = 51 ; Dts = 1min ; Phys Opt = 4 ; PBL Opt = 5 ; Cu Opt = 6

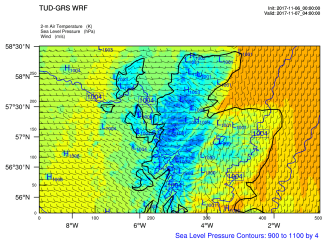
TUD-GRS WRF
Init: 2017-11-6\6_00:00:00
Valid: 2017-11-6?_34:00:00
2-m Air Temperature (K)
Sea Level Pressure (hPa)
Wind (m/s)
58°30'N
58°N
57°30'N
57°N
56°30'N
56°N
8°W
6°W
4°W
2°W
Sea Level Pressure Contours: 900 to 1100 by 4
2-m Air Temperature (K)
270 272 274 276 278 280 282 284 286 288 290
OUTPUT FROM WRF V3.9.1 MODEL
IM1 = 500 ; DM = 281 ; Levels = 51 ; Dts = 1min ; Phys Opt = 4 ; PBL Opt = 5 ; Cu Opt = 6

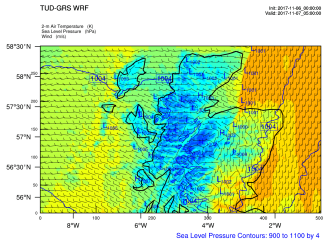
TUD-GRS WRF
Init: 2017-11-6\6_00:00:00
Valid: 2017-11-6?_35:00:00
2-m Air Temperature (K)
Sea Level Pressure (hPa)
Wind (m/s)
58°30'N
58°N
57°30'N
57°N
56°30'N
56°N
8°W
6°W
4°W
2°W
Sea Level Pressure Contours: 900 to 1100 by 4
2-m Air Temperature (K)
270 272 274 276 278 280 282 284 286 288 290
OUTPUT FROM WRF V3.9.1 MODEL
IM1 = 500 ; DM = 281 ; Levels = 51 ; Dts = 1min ; Phys Opt = 4 ; PBL Opt = 5 ; Cu Opt = 6

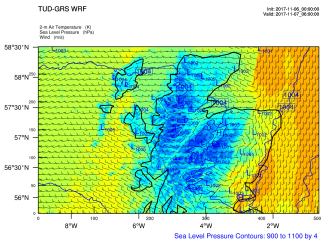
TUD-GRS WRF
Init: 2017-11-6\6_00:00:00
Valid: 2017-11-6?_36:00:00
2-m Air Temperature (K)
Sea Level Pressure (hPa)
Wind (m/s)
58°30'N
58°N
57°30'N
57°N
56°30'N
56°N
8°W
6°W
4°W
2°W
Sea Level Pressure Contours: 900 to 1100 by 4
2-m Air Temperature (K)
270 272 274 276 278 280 282 284 286 288 290
OUTPUT FROM WRF V3.9.1 MODEL
IM1 = 500 ; DM = 281 ; Levels = 51 ; Dts = 1min ; Phys Opt = 4 ; PBL Opt = 5 ; Cu Opt = 6

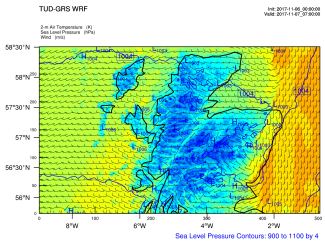
TUD-GRS WRF
Init: 2017-11-6\6_00:00:00
Valid: 2017-11-6?_37:00:00
2-m Air Temperature (K)
Sea Level Pressure (hPa)
Wind (m/s)
58°30'N
58°N
57°30'N
57°N
56°30'N
56°N
8°W
6°W
4°W
2°W
Sea Level Pressure Contours: 900 to 1100 by 4
2-m Air Temperature (K)
270 272 274 276 278 280 282 284 286 288 290
OUTPUT FROM WRF V3.9.1 MODEL
IM1 = 500 ; DM = 281 ; Levels = 51 ; Dts = 1min ; Phys Opt = 4 ; PBL Opt = 5 ; Cu Opt = 6

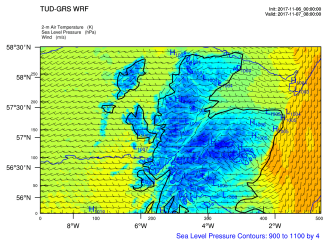
TUD-GRS WRF
Init: 2017-11-6\6_00:00:00
Valid: 2017-11-6?_38:00:00
2-m Air Temperature (K)
Sea Level Pressure (hPa)
Wind (m/s)
58°30'N
58°N
57°30'N
57°N
56°30'N
56°N
8°W
6°W
4°W
2°W
Sea Level Pressure Contours: 900 to 1100 by 4
2-m Air Temperature (K)
270 272 274 276 278 280 282 284 286 288 290
OUTPUT FROM WRF V3.9.1 MODEL
IM1 = 500 ; DM = 281 ; Levels = 51 ; Dts = 1min ; Phys Opt = 4 ; PBL Opt = 5 ; Cu Opt = 6

G

WIND SPEED AT HUB HEIGHT - CASE STUDY I - MYNNWP

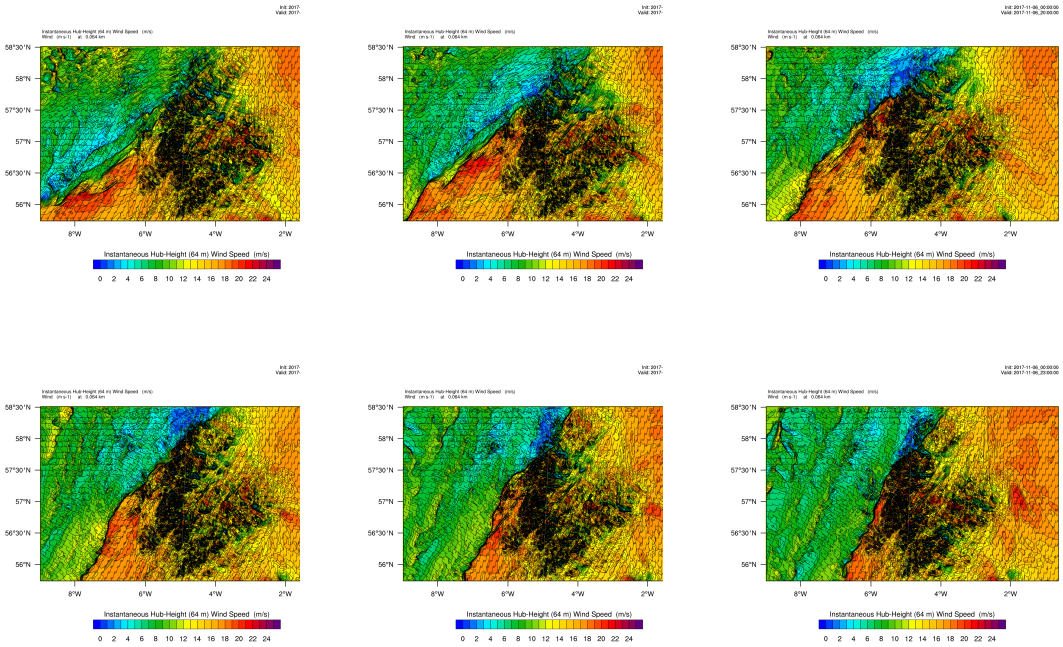

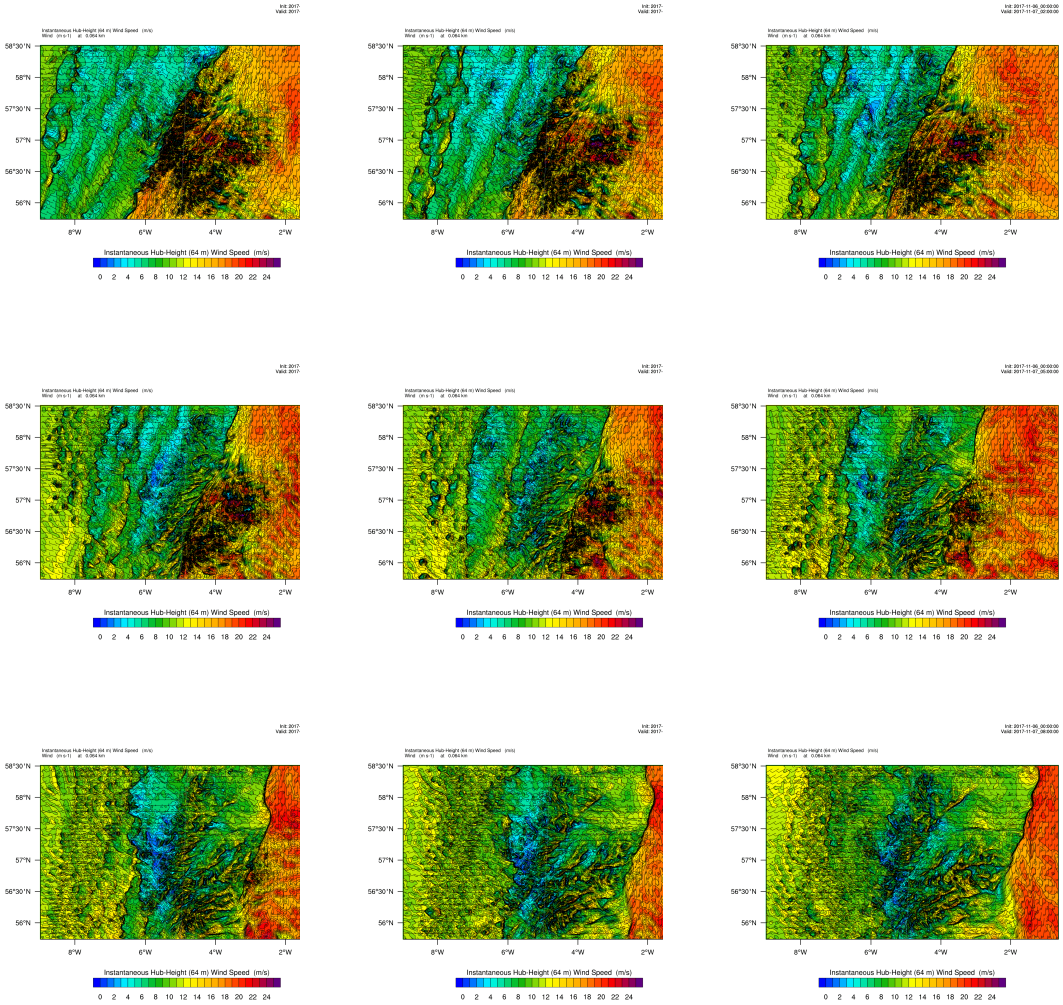
Init: 2017-
Valid: 2017-
Instantaneous Hub-Height (64 m) Wind Speed (m/s)
Wind (m s-1) at 0.064 km
58°30'N
58°N
57°30'N
57°N
56°30'N
56°N
8°W
6°W
4°W
2°W
Instantaneous Hub-Height (64 m) Wind Speed (m/s)
0 2 4 6 8 10 12 14 16 18 20 22 24
Init: 2017-11-30_00:00:00
Valid: 2017-11-07_00:00:00
Init: 2017-11-30_00:00:00
Valid: 2017-11-07_06:00:00
Init: 2017-11-30_00:00:00
Valid: 2017-11-07_12:00:00
Init: 2017-11-30_00:00:00
Valid: 2017-11-07_18:00:00

H

WIND SPEED AT SURFACE - CASE STUDY II - YSU

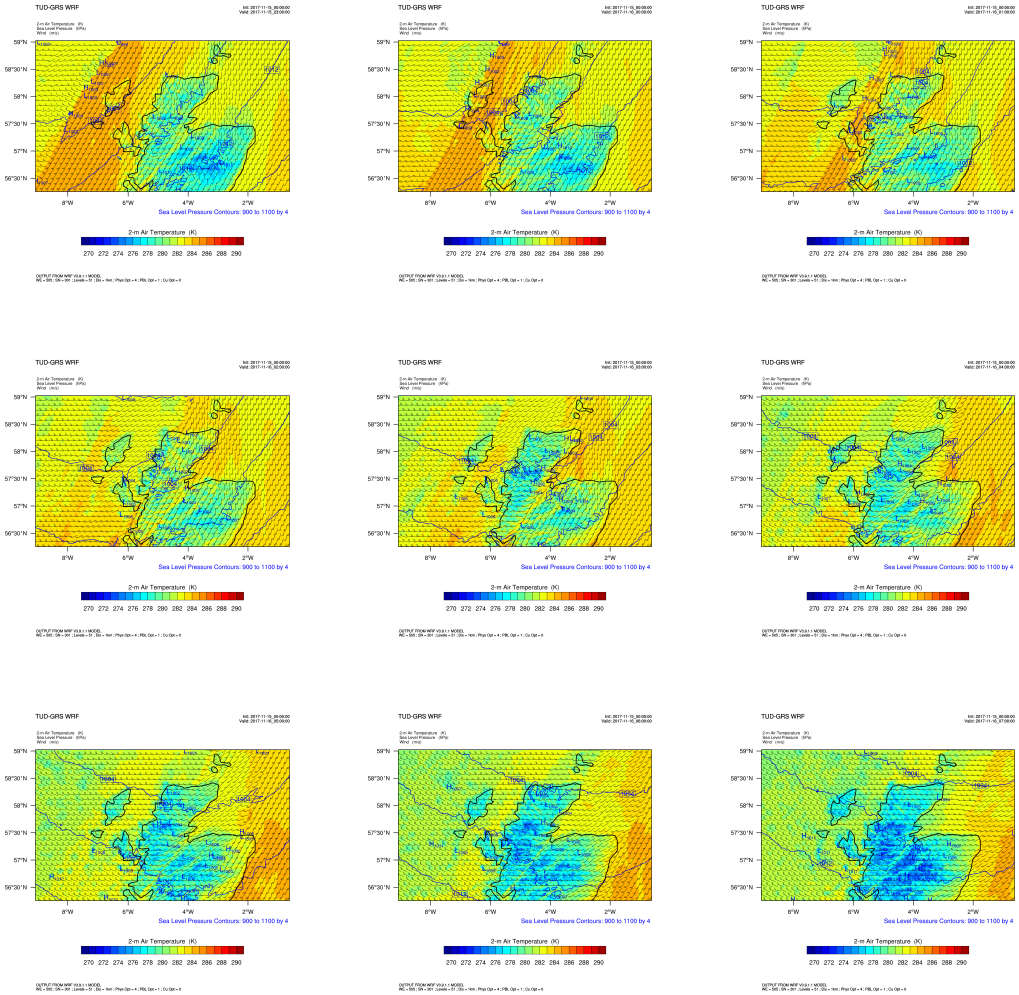

I

WIND SPEED AT HUB HEIGHT - CASE STUDY II - YSU

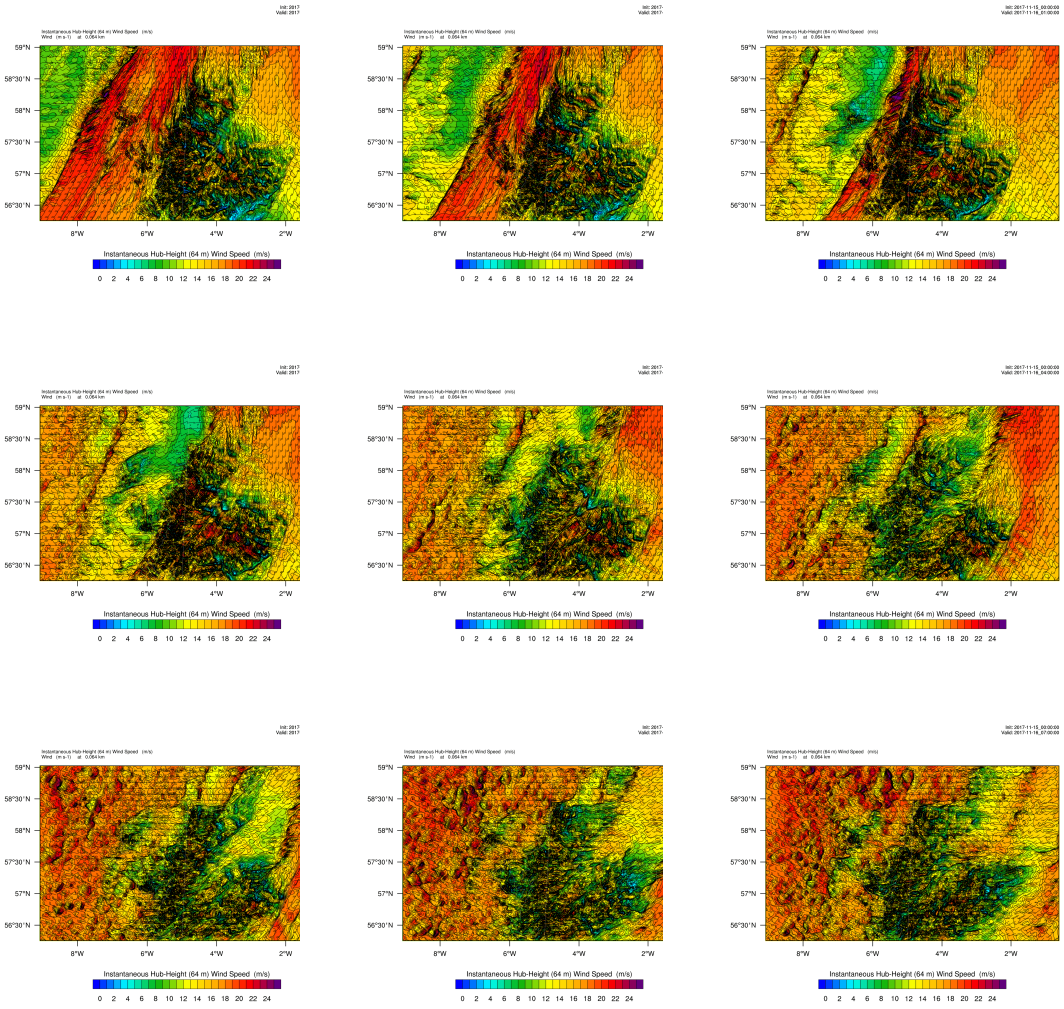

J
Wind speed at surface - Case Study II - MYNN

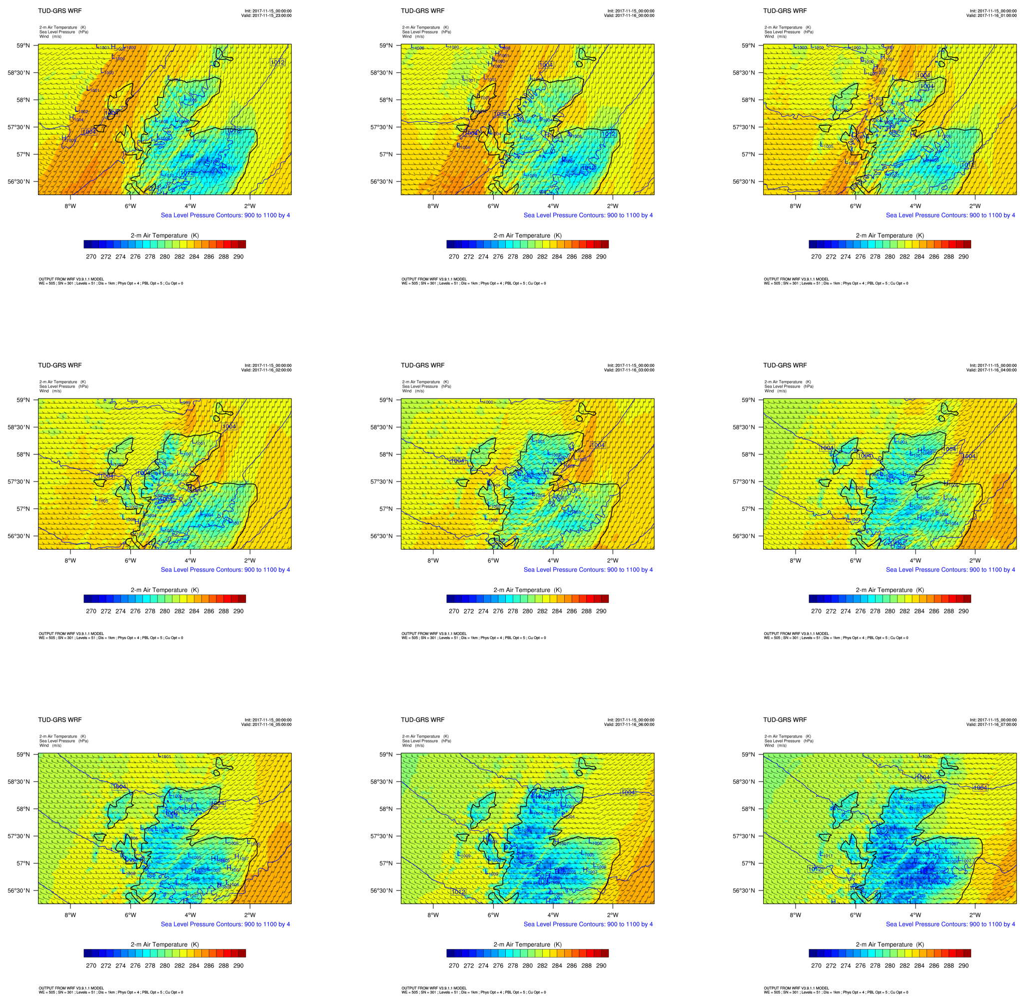

K

WIND SPEED AT HUB HEIGHT - CASE STUDY II - MYNN

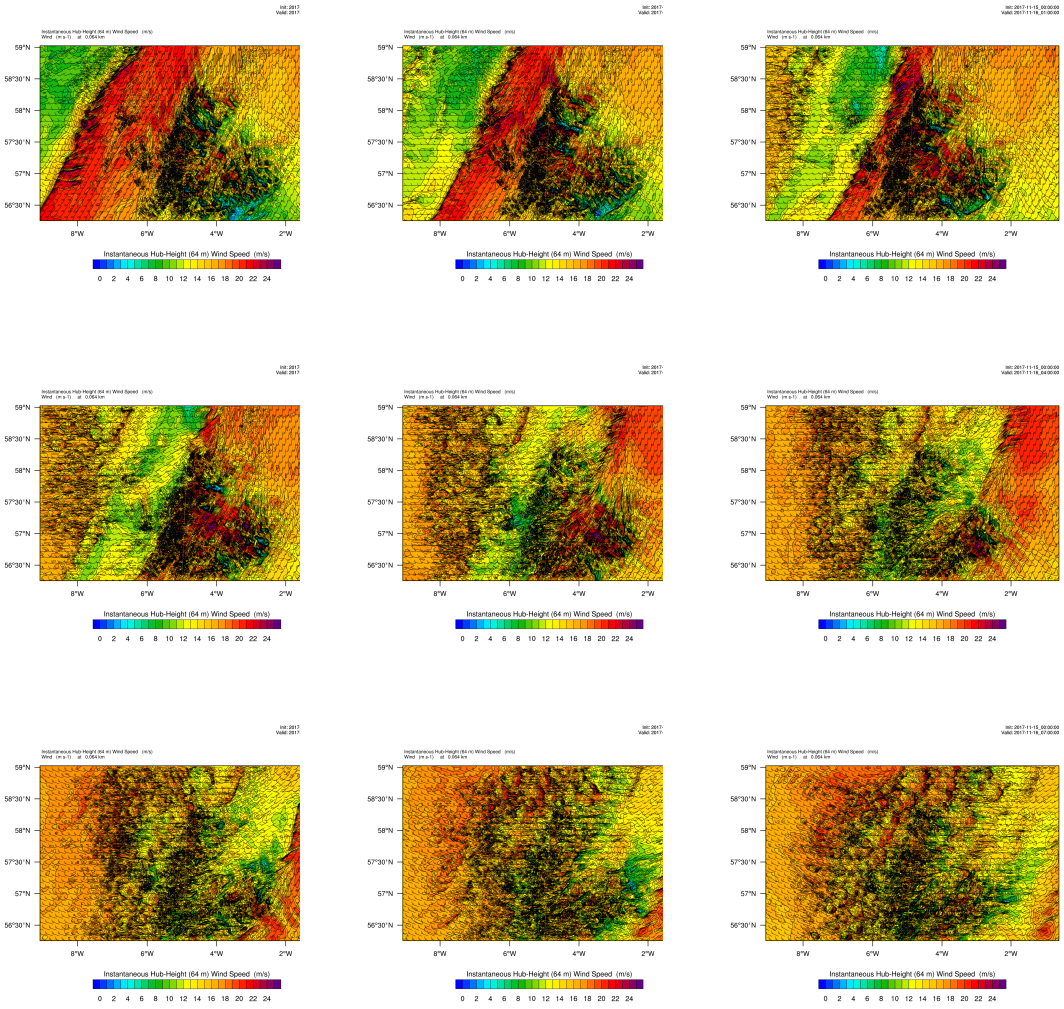

L

WIND SPEED AT SURFACE - CASE STUDY II - MYNNWP

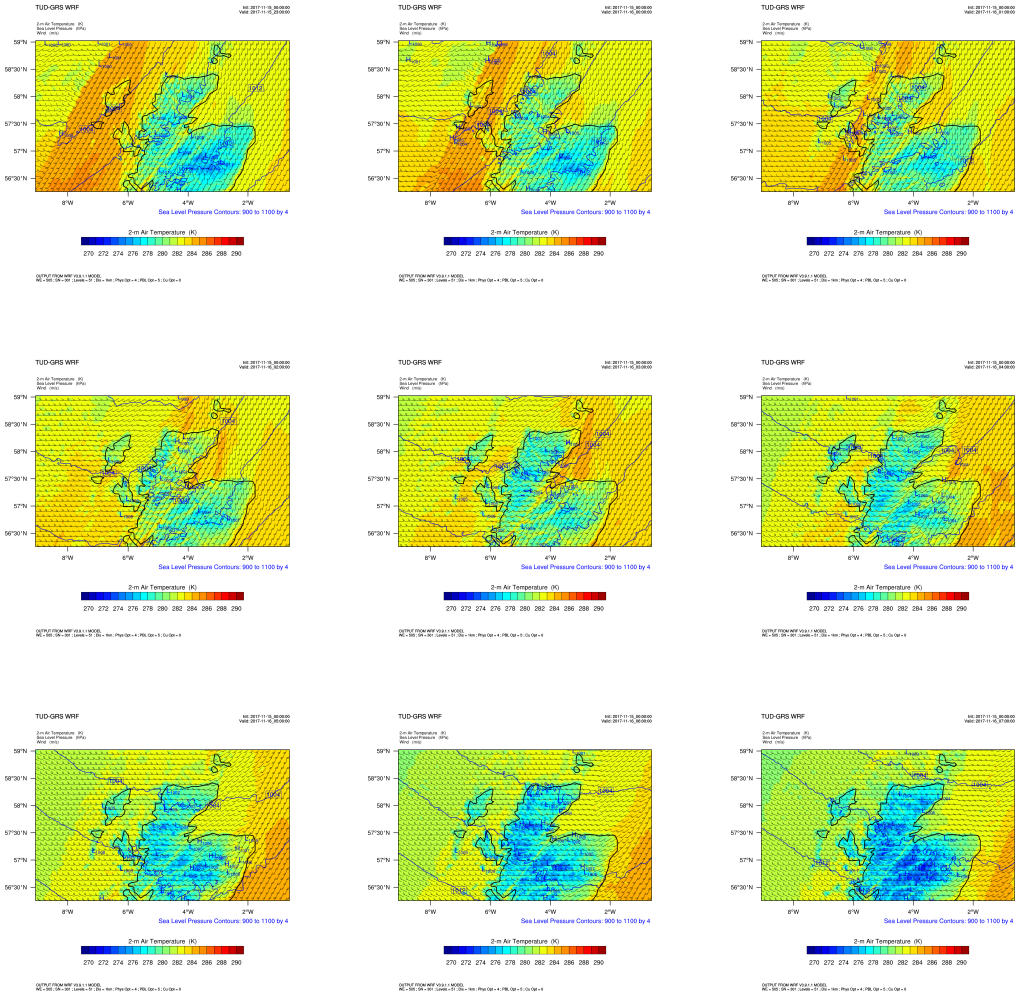

M

WIND SPEED AT HUB HEIGHT - CASE STUDY II - MYNNWP

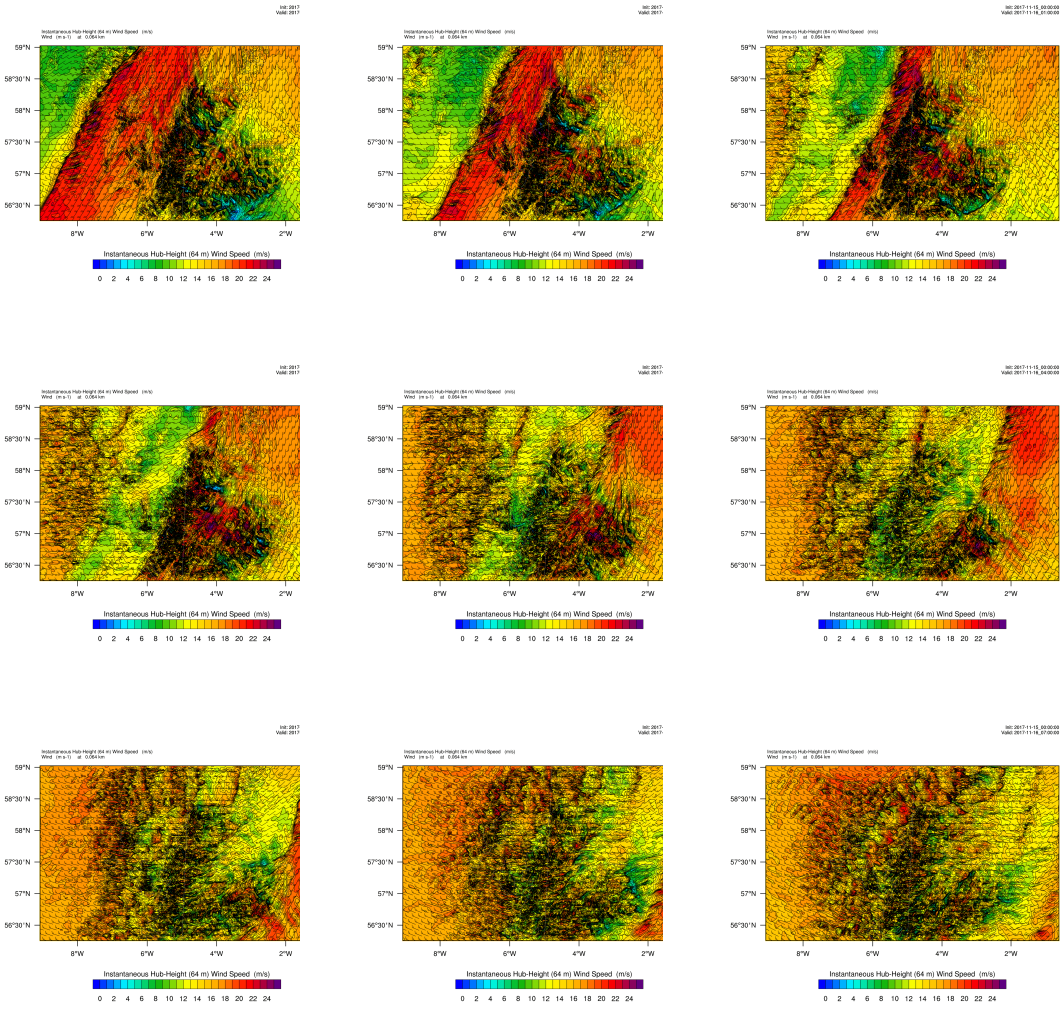

BIBLIOGRAPHY

Edgar L Andreas, Kerry J Claffey, and Aleksander P Makshtas. Low-level Atmospheric Jets and Inversions over the Western Weddell Sea. *Boundary Layer Meteorology*, 97:459–486, 2000.

P. Baas, F. C. Bosveld, and H. Klein Baltink. A Climatology of Nocturnal Low-Level Jets at Cabauw. *Journal of Applied Meteorology and Climatology*, 48:1627–1642, 2009.

Erin Baker. Blackdog LiDAR - Installation Report. Technical report, Oldbaum, sep 2016.

R M Banta, R K Newsom, J K Lundquist, Y I Pichugina, R I Coulter, and L Mahrt. Nocturnal Low-Level Jet Characteristics over Kansas during Cases-99. *Boundary-Layer Meteorology*, 105(2):221–252, 2002.

Alfred K. Blackadar. Boundary Layer Wind Maxima and Their Significance for the Growth of Nocturnal Inversions. *Bulletin of the American Meteorological Society*, 38(5):283–290, 1957. ISSN 0003-0007. doi: 10.1175/1520-0477-38.5.283. URL http://journals.ametsoc.org/doi/10.1175/1520-0477-38.5.283.

K. A. Browning and T. W. Harrold. Air motion and precipitation growth at a cold front. *Quarterly Journal of the Royal Meteorological Society*, 96:369–389, 1970.

K. A. Browning and C. W. Pardoe. Structure of low-level jet streams ahead of mid-latitude cold fronts. *Quarterly Journal of the Royal Meteorological Society*, 99:619–638, 1973.

K. A. Browning, D. Jerrett, J. Nash, T. Oakly, and N. M. Roberts. Cold frontal structure derived from radar wind profilers. *Meterology Applied*, 5:67–74, 1998.

Robert Creighton. Go fly a kite. *IEEE Spectrum*, 49(12):46–51, 2012.

H. de Coninck, A. Revi, M. Babiker, P. Bertoldi, M. Buckeridge, A. Cartwright, W. Dong, J. Ford, S. Fuss, JC. Hourcade, D. Ley, R. Mechler, P. Newman, A. Revokatova, S. Schultz, L. Steg, and T. Sugiyam. *Global warming of 1.5°C. An IPCC Special Report on the impacts of global warming of 1.5°C above pre-industrial levels and related global greenhouse as emission pathways, in the context of strengthening the global response to the threat of climate change, sustainable development, and efforts to eradicate poverty*, chapter Strengthening and implementing the global response, pages 313–443. In Press, 2018.

Dave Donovan. Lidar Techniques. Lecture notes, 2018.

James D Doyle and Thomas T Warner. A Carolina Coastal Low-Level Jet during GALE IOP 2. *Monthly Weather Review*, 119:2412–2428, 1991.

Stefan Emeis. *Surface-Based Remote Sensing of the Atmospheric Boundary Layer*. Springer, 2011.

C. Ferreira, J. Gama, L. Matias, A. Botterud, and J. Wang. A survey on wind power ramp forecasting. Technical report, Argonne National Laboratory, 2010.

Anna C. Fitch, Joseph B. Olson, Julie K. Lundquist, Jimy Dudhia, Alok K. Gupta, John Michalakes, and Idar Barstad. Local en mesoscale impacts of wind farms as parameterized in a mesoscale nwp model. *Monthly Weather Review*, 140:3017–3038, September 2012.

Daniel Fraile and Ariola Mbistrova. Wind in power 2017. Technical report, Wind Europe, 2017.

J. R. Garratt. Review: the atmospheric boundary layer. *Earth-Science Reviews*, 37:89–134, 1994.

Nathalie Ghazi. Krachtigste windmolen ter wereld in Aberdeen Bay geïnstalleerd, apr 2018. URL https://intranet.vattenfall.com/nl/news/2018/04/worlds-most-powerful-wind-turbine-installed-in-aberdeen-bay/.

Julia Gottschall, Brian Gribben, Detlef Stein, and Ines Würth. Floating lidar as an advanced offshore wind speed measurement technique: current technology status and gap analysis in regard to full maturity. *Wiley Interdisciplinary Reviews: Energy and Environment*, 6(5), 2017.

Erich Hau. *Wind Turbines*. Springer, 2006.

Karl Hennermann and Anabelle Guillory. What are the changes from era-interim to era5. website, May 2019. URL https://confluence.ecmwf.int/pages/viewpage.action?pageId=74764925.

Song-You Hong, Yign Noh, and Jimy Dudhia. A new vertical diffusion package with an explicit treatment of entrainment processes. *Monthly Weather Review*, 134:2318–2341, 2006.

Xiao-Ming Hu, John W. Nielsen-Gammon, and Fuqing Zhang. Evaluation of three planetary boundary layer schemes in the wrf model. *Journal of Applied Meteorology and Climatology*, 49:1831–1844, 2010.

Jo Hutchinson. Edinbane, isle of skye. website, October 2014. URL https://corporate.vattenfall.co.uk/projects/operational-wind-farms/edinbane-isle-of-skye/.

Chandrika Kamath. Understanding wind ramp events through analysis of historical data. In *IEEE PES Transmission and Distribution Conference and Expo*. Lawrence Livermore National Laboratory, April 2010.

Chandrika Kamath. Associating weather conditions with ramp events in wind power generation. In *IEEE Power Systems Conference and Exposition*. Lawrence Livermore National Laboratory, March 2011.

Gary Lackmann. *Midlatitude Synoptic Meteorology*. American Meteorologial Society, 2011.

Eric Loth, Adam Steele, Brian Ichter, Michael Selig, and Patrick Moriarty. Segmented ultralight pre-aligned rotor for extreme-scale wind turbines. In *50th AIAA Aerospace Sciences Meeting including the New Horizons Forum and Aerospace Exposition*, 2012.

Eric Loth, Adam Steele, Chao Qin, Biran Ichter, Michael S. Selig, and Patrick Moriarty. Downwind pre-aligned rotors for extreme-scale wind turbines. *Wind Energy*, 20:1241–1259, 2017.

V. Masson-Delmotte, P. Zhai, H. O. Pörtner, D. Robert, J. Skea, P. R. Shukla, A. Pirani, W. Moufouma-Okia, C. Péan, R. Pidcock, S. Connors, J. B. R. Matthews, Y. Chen, X. Zhou, M. I. Gomis, E. Lonnoy, T. Maycock, M. Tignor, and T. Waterfield (eds.). *Global warming of 1.5°C. An IPCC Special Report on the impacts of global warming of 1.5°C above pre-industrial levels and related global greenhouse as emission pathways, in the context of strengthening the global response to the threat of climate change, sustainable development, and efforts to eradicate poverty*, chapter Summary for Policymakers, page 32. World Meteorological Organization, 2018.

MetOffice. Daily weather summary: November 2017, December 2017a. URL https://digital.nmla.metoffice.gov.uk/.

MetOffice. Midas: Uk hourly weather observation data. website, 2017b.

MetOffice. Search for met office midas stations. website, 2018. URL http://archive.ceda.ac.uk/midas_stations/.

Mikio Nakanishi and Hiroshi Niino. An improved mellor-yamada level-3 model with condensation physics: Its design and verification. *Boundary-Layer Meteorology*, 112:1–31, 2004.

Mikio Nakanishi and Hiroshi Niino. An improved mellor-yamada level-3 model: Its numerical stability and application to a regional prediction of advection fog. *Boundary-Layer Meteorology*, 119:397–407, 2006.

Joseph B. Olson, Jaymes S. Kenyon, Wayne A. Angevine, John M. Brown, Mariusz Pagowski, and Kay Suselj. A description of the mynn-edmf scheme and the coupling to other components in wrf-arw. Technical report, National Oceanic and Atmospheric Administration, 2019.

Thomas R Parish. Forcing of the Summertime Low-Level Jet along the California Coast. *Journal of Applied Meteorology*, 39(12), 2000.

Raffi Sevlian and Ram Rajagopal. Detection and statistics of wind power ramps. *IEEE Transactions on Power Systems*, 28(4):3610–3620, 2013.

Alan Shapiro and Evgeni Fedorovich. Analytical description of a nocturnal low-level jet. *Quarterly Journal of the Royal Meteorological Society*, 136(650):1255–1262, 2010. ISSN 00359009. doi: 10.1002/qj.628.

Hyeyum Hailey Shin and Song-You Hong. Intercomparison of planetary boundary-layer parametrizations in the wrf model for a single day from cases-99. *Boundary-Layer Meteorology*, 139:261–281, 2011.

William C. Skamarock, Joseph B. Klemp, Jimy Dudhia, David O. Gill, Dale M. Barker, Michael G. Duda, Xiang-Yu Huang, Wei Wang, and Jordan G. Powers. A description of the advanced research wrf version 3. Technical report, Mesoscale and Microscale Meteorology Division, National Center for Atmospheric Research (NCAR), 2008.

Linda Speight. Radar coverage and suitability for flood forecasting in scotland. website, November 2014.

David J. Stensrud. *Parameterization Schemes*. Cambridge University Press, 2007.

Brandon Storm, Jimy Dudhia, Sukanta Basu, Andy Swift, and Tian Giammanco. Evaluation of the weather research and forecasting model on forecasting low-level jets: Implications for wind energy. *Wind Energy*, 12:81–90, 2009.

Roland Stull. *Practical Meteorology*. Universiy of British Columbia, 2017.

Thomson. Cold front diagram, 2007. URL http://www.athensgaweather.com/meteorology-101-pressure-fronts/.

Alan J. Thorpe and Trevor H. Guymer. The nocturnal jet. *Quarterly Journal of the Royal Meteorological Society*, 103(438):633–653, 1977. ISSN 1477870X. doi: 10.1002/qj.49710343809.

Christine Unal. Radar meteorology - lecture 1. Course: Atmospheric Observation, 2018.

Vattenfall. European Offshore Wind Deployment Centre, nov 2016. URL https://corporate.vattenfall.co.uk/projects/wind-energy-projects/european-offshore-wind-deployment-centre/about-the-project/.

Axelle Viré. Introduction to wind energy: Wind turbines. Lecture slides, 2018.

Mark Vogan. Europe: Classic icelandic low/azores high pressure pattern. website, July 2016. URL http://www.markvoganweather.com/2016/07/06/europe-classic-icelandic-lowazores-high-pressure-pattern/.

Barry White. Babcock FORECAST Deployment. Technical report, Babcock Energy & Marine Technology, nov 2016.

ZephIR. *ZephIR CSV Files: A User's Guide*. Zephir Ltd., 1 edition, dec 2012.

Udo Zillmann and Philip Bechtle. *Airborne Wind Energy*, chapter Emergence and Economic Dimension of Airborne Wind Energy, pages 1–25. Springer, 2018.